







# Methods—Understanding Porous Electrode Impedance and the Implications for the Impedance Analysis of Li-Ion Battery Electrodes

Robert Morasch,<sup>1,z</sup>  Josef Keilhofer,<sup>1,2</sup>  Hubert A. Gasteiger,<sup>1</sup>  and Bharatkumar Suthar<sup>3</sup> 

<sup>1</sup>Chair of Technical Electrochemistry, Department of Chemistry and Catalysis Research Center, Technical University of Munich, Munich, Germany

<sup>2</sup>current address: Department of Mechanical Engineering, Institute for Machine Tools and Industrial Management (iwb), Technical University of Munich, Munich, Germany

<sup>3</sup>Department of Chemical Engineering, Indian Institute of Technology Bombay, Mumbai 400076, India

Two of the main factors influencing the performance of Li-ion battery (LIB) electrodes are the kinetic losses due to the charge transfer resistance of the active material ( $R_{ct}$ ) and the ionic transport resistance in the electrolyte phase within the electrode pores ( $R_{ion}$ ). Seeking to increase the energy density of LIBs, ever higher active material loadings are applied, resulting in thicker electrodes for which  $R_{ion}$  becomes dominant. As electrochemical impedance spectroscopy is commonly used to quantify  $R_{ct}$  of electrodes, understanding the impact of  $R_{ion}$  on the impedance response of thick electrodes is crucial. By use of a simplified transmission line model (TLM), we simulate the impedance response of electrodes as a function of electrode loading. This will be compared to the impedance of graphite anodes (obtained using a micro-reference electrode), demonstrating that their impedance response varies from purely kinetically limited at  $0.6 \text{ mAh cm}^{-2}$  to purely transport limited at  $7.5 \text{ mAh cm}^{-2}$ . We then introduce a simple method with which  $R_{ct}$  and  $R_{ion}$  can be determined from the electrode impedance, even under transport limited conditions. Finally, we show how the initially homogenous ionic current distribution across porous electrodes under kinetically limited conditions becomes severely inhomogeneous under transport limited conditions.

© 2021 The Author(s). Published on behalf of The Electrochemical Society by IOP Publishing Limited. This is an open access article distributed under the terms of the Creative Commons Attribution Non-Commercial No Derivatives 4.0 License (CC BY-NC-ND, <http://creativecommons.org/licenses/by-nc-nd/4.0/>), which permits non-commercial reuse, distribution, and reproduction in any medium, provided the original work is not changed in any way and is properly cited. For permission for commercial reuse, please email: [permissions@iopublishing.org](mailto:permissions@iopublishing.org). [DOI: [10.1149/1945-7111/ac1892](https://doi.org/10.1149/1945-7111/ac1892)]



Manuscript submitted May 21, 2021; revised manuscript received July 1, 2021. Published August 16, 2021.

Analyzing the electrochemical impedance spectroscopy (EIS) spectra of electrochemical cells and electrodes requires an in-depth knowledge of the underlying kinetic and transport processes and their appropriate representation via an equivalent circuit model. The perhaps most commonly used circuit element to describe the response of electrochemical systems is the so-called  $R/C$  element, i.e., the parallel arrangement of a resistor and a capacitor. This element can be used to describe a multitude of interfaces, most prominently the electrochemical interface between an electrode and an ionically conductive electrolyte, e.g., the interface between a battery active material and the electrolyte. When describing the electrochemically active surface area of the active material with an  $R/C$  element, the resistor represents the kinetic resistance for the faradaic charge transfer reaction and the capacitor models the capacitive effect arising from the electrochemical double layer forming at the interface of the electrochemically responsive electrode material surfaces (i.e., the active material and the conductive carbon) and the ion conducting electrolyte.<sup>1</sup> The resulting spectrum for such an  $R/C$  circuit element in a Nyquist plot is a semicircle, with a diameter that corresponds to the resistance  $R$  and that spans over a frequency range that is in part also defined by the capacitive element  $C$ . As actual electrochemical systems generally do not show a perfect capacitive behavior and are generally better described by a so-called constant phase element  $Q$ , the  $R/C$  element (resulting in a semicircle in a Nyquist plot) is typically replaced by an  $R/Q$  element that results in a slightly depressed semicircle.

In addition to the charge transfer resistance ( $R_{ct}$ ) and the electrode capacitance ( $Q_{dl}$ ), the electrode impedance of porous Li-ion battery electrodes also depends on the ionic resistance within the electrolyte phase contained in the pores of the electrode ( $R_{ion}$ ). For this reason, the quantification of the charge transfer resistance of a LIB electrode and its change over the course of cycling from impedance measurements is not straightforward and requires a more refined equivalent circuit model. A commonly used representation of the impedance of a

porous electrode is given by the so-called transmission line model (TLM), which in its simplified form is here composed of a resistive path (with  $R_{ion}$  as the sum of the resistance elements  $r_{ion}$ , stemming from the electrolyte in the pores of the electrode) as well as of  $r_{ct}/q_{dl}$  elements that act as local current source or sink to the resistive path (see top part of Fig. 1). The  $r_{ct}/q_{dl}$  elements cumulatively give rise to the overall charge transfer resistance ( $R_{ct}$ ) and the overall double layer capacitance ( $Q_{dl}$ ), as described in the caption of Fig. 1. Other possible contributions to the electrode impedance are not being considered for the following reasons: (i) electrical resistances across the electrode are typically negligible compared to ionic resistances, particularly for graphite anodes that are in the focus of this study<sup>2</sup>; (ii) solid and electrolyte Warburg diffusion elements (in the electrodes and in separator) are not expected to influence the impedance spectra within the here examined frequency region<sup>3,4</sup>; (iii) the separator resistance, since it only results in a constant high-frequency offset of the spectra. A review of EIS applications including different circuit elements can be found in Ref. 5.

Driven by the demand to increase the energy density of LIBs, increasingly higher active material (AM) loadings (in units of  $\text{mg}_{AM} \text{ cm}^{-2}$ ), corresponding to higher areal capacities ( $C_{areal}$ , in units of  $\text{mAh cm}^{-2}$ , not to be confused with the previously defined capacitance  $C$ ), are being employed, since this leads to a lower mass fraction of inactive materials (current collectors, separators, current tabs) and therefore also lower cost.<sup>6,7</sup> Conceptually, a doubling of the areal capacity, assuming the same electrode composition and morphology (i.e., porosity and tortuosity), has the following consequences: (i) a doubling of the material surface area that is in contact with the electrolyte, thus a doubling of the electrode capacitance (i.e.,  $Q_{dl} \propto C_{areal}$ ); (ii) a doubling of the active material surface area, resulting in a halving of the charge transfer resistance (i.e.,  $R_{ct} \propto 1/C_{areal}$ ); and, (iii) a doubling of the electrode thickness, resulting in a doubling of the ionic resistance (i.e.,  $R_{ion} \propto C_{areal}$ ). Figure 1 shows a schematic of how the increase in active material loading (i.e., of areal electrode capacity  $C_{areal}$  which in turn scales with electrode thickness) affects the two resistances. Starting at an arbitrary active material loading (referred to as “Loading I”) with a

<sup>z</sup>E-mail: [robert.morasch@tum.de](mailto:robert.morasch@tum.de)

ratio of the charge transfer resistance over the ionic resistance of  $R_{ct}/R_{ion} \equiv A/B$ , doubling the loading effectively doubles the ionic resistance and halves the charge transfer resistance, resulting in  $R_{ct}/R_{ion} = (1/2)/2 \times A/B$  for the electrode with a two-fold higher active material loading (“Loading 2”). Further increasing the active material loading by a factor of 3 and 4 results in  $R_{ct}/R_{ion} = (1/3)/3 \times A/B$  and  $R_{ct}/R_{ion} = (1/4)/4 \times A/B$ , respectively. In other words, a 4-fold increase in areal capacity is expected to lead to a 16-fold decreased  $R_{ct}/R_{ion}$  value.

As Li-ion batteries make use of an intercalation reaction, i.e., the lithium is stored in the active material, lithium ions eventually have to reach the interface of the electrode with the current collector (CC) (right-hand side of Fig. 1) during the lithiation of the active material particles, or have to be transported through the electrode and the separator to the opposing separator/electrode interface (left-hand side) during delithiation. For *very thin electrodes* (i.e., for very low active material loadings and areal capacities),  $R_{ion}$  is negligible and the electrode impedance is dominated by  $R_{ct}$  (furtheron referred to as *kinetically limited*). On the other hand, for high loaded *thick electrodes* (i.e., for high areal capacities),  $R_{ion}$  will dominate the electrode impedance due to the increased ion conduction path length through the electrode and the simultaneously decreased  $R_{ct}$  (furtheron referred to as *transport limited*). Which of the two limiting cases become dominant for a given active material loading (or areal capacity) is a question addressed in this work. The impact of the ion conduction resistance through the porous electrodes on EIS spectra has previously been studied, but these earlier studies neglected the influence of low  $R_{ct}/R_{ion}$  values on the mathematical response of the transmission line model,<sup>8–12</sup> so that these findings are only relevant for low active material loadings. Therefore, we have extended this analysis to the low  $R_{ct}/R_{ion}$  regime that, as we will show, is relevant for LIB graphite anodes with currently used areal capacities of  $\sim 3$  mAh cm<sup>-2</sup> and beyond.

To understand the transition of the impedance response of a LIB electrode from the kinetically limited regime at low active material loadings (i.e., at high  $R_{ct}/R_{ion}$  values) to the transport limited regime at high active material loadings (i.e., at low  $R_{ct}/R_{ion}$  values), we first simulate the EIS spectra using the transmission line model shown in Fig. 1 for different  $R_{ct}/R_{ion}$  values. We will show how the impedance spectrum changes from exhibiting an  $R_{ct}$ -dominated semicircle at high  $R_{ct}/R_{ion}$  values to a non-semicircle shaped spectrum at low  $R_{ct}/R_{ion}$  from which the determination of the charge transfer resistance requires additional considerations. We then compare these simulated spectra to experimentally obtained impedance spectra of LIB graphite anodes with widely varying graphite loadings, corresponding to areal capacities of  $C_{areal} = 0.6$ – $7.5$  mAh cm<sup>-2</sup>, showing that their impedance response indeed varies from purely kinetically limited (for  $0.6$  mAh cm<sup>-2</sup>) to purely transport limited (for  $7.5$  mAh cm<sup>-2</sup>). An additional current distribution analysis gives insight into the change in current homogeneity throughout the electrode. Lastly we demonstrate how to analyze these impedance spectra without the need for a fitting software to give the user the ability to analyze and deconvolute  $R_{ct}$  from the electrode impedance spectrum.

## Experimental

**Slurry preparation and drying.**—Graphite (T311, Timcal,  $19 \mu\text{m}$  D50,  $3 \text{ m}^2 \text{ g}^{-1}$ ) and polymer binder (polyvinylidene fluoride (PVDF), Kynar, Arkema) at a ratio of 95:5 (wt:wt) were mixed with N-Methyl-2-pyrrolidone (NMP, Sigma Aldrich, anhydrous, 99.5%) at a solid:liquid ratio of 5:4 (wt:wt) in a planetary mixer (Thinky ARV-310) at 2000 rpm for five minutes. The prepared graphite slurries were coated onto a copper current collector foil (MTI,  $12 \mu\text{m}$ ) attached to a glass plate using a gap bar coater (RK PrintCoat Instruments, UK) at wet film thicknesses of  $30 \mu\text{m}$ ,  $100 \mu\text{m}$ ,  $200 \mu\text{m}$ , and  $450 \mu\text{m}$  to achieve areal capacities of  $0.6$ ,  $1.5$ ,  $2.9$ , and  $7.5$  mAh cm<sup>-2</sup>, respectively (referenced to a nominal

graphite capacity of  $350 \text{ mAh g}_G^{-1}$ ), and dried in an oven at  $50 \text{ }^\circ\text{C}$ . The dried electrodes were punched out to a diameter of  $10.95 \text{ mm}$  (equating to an area of  $\sim 0.94 \text{ cm}^2$ ) using an electrode punch (Hohsen Corp. OSAKA, Japan), and compressed in a press using a pressure of  $\sim 100 \text{ MPa}$ . The specifications of the graphite electrodes with regards to graphite loading (in  $\text{mg}_G \text{ cm}^{-2}$ ), electrode thickness, and electrode porosity are summarized in Table 1. Densities used for the porosity calculations were  $2.26 \text{ g cm}^{-3}$  for graphite and  $1.77 \text{ g cm}^{-3}$  for PVDF.

**Cell assembly, formation and impedance measurement.**—For electrochemical impedance analysis, a three-electrode cell setup (Swagelok® T-cell) with a gold-wire reference electrode (GWRE; described in more detail in Fig. 1b in Ref. 13) was used. The cells were built inside an argon filled glove box (MBraun,  $25 \text{ }^\circ\text{C} \pm 1 \text{ }^\circ\text{C}$ , oxygen and water content  $< 0.1$  ppm, Ar 5.0, Westfalen). All cell parts were dried at  $120 \text{ }^\circ\text{C}$  in a vacuum oven (Büchi, Switzerland) for 8 h before being transferred into the glovebox.

The cells were assembled with a graphite working electrode, two porous glass fiber separators with a diameter of  $11 \text{ mm}$  (VWR,  $250 \mu\text{m}$  uncompressed thickness, 90% porosity), and a counter electrode consisting of a free-standing graphite electrode that was firmly attached to the metallic lithium foil ( $0.45 \text{ mm}$  thickness and  $11 \text{ mm}$  diameter, Rockwood Lithium), as described in Ref. 14  $80 \mu\text{l}$  of LP57-2 electrolyte (1 M LiPF<sub>6</sub> in EC:EMC 3:7 (wt:wt) + 2 wt% VC, battery grade, BASF) were added to the cells.

Using a potentiostat (Bio-Logic Science Instruments, France), the gold-wire reference electrode was lithiated at  $150 \text{ nA}$  for 1 h via the counter electrode in a temperature-controlled chamber ( $25 \text{ }^\circ\text{C}$ , Binder). The cycling protocol started with a 3 h open circuit voltage phase to allow for complete wetting of the electrode. Two formation cycles for the graphite working electrode were performed galvanostatically at C/10 (referenced to a nominal specific capacity of  $350 \text{ mAh g}_G^{-1}$ ) between 2V and 40 mV vs Li<sup>+</sup>/Li. The electrode was then brought to 50% state of charge (SOC) at C/10. Potentiostatic electrochemical impedance measurements were performed at open circuit voltage (OCV) from 30 kHz to 0.1 Hz and with an excitation of 10 mV; the use of the micro-reference electrode (i.e., the GWRE) allowed for a rigorous determination of the impedance response of the graphite electrode.

**Current distribution analysis.**—The theoretical background for the current distribution analysis can be found in the Appendix.

**Data simulation and fitting.**—Impedance simulation and fitting was performed with a MATLAB-based application (“EIS Breaker,” © J. Landesfeind) based on the `fminsearch` MATLAB function using a Nelder-Mead simplex algorithm and modulus weighing. For all data fitting, only the value of  $R_{ion}$  was fixed, while the remaining parameters ( $R_{ct}$ ,  $Q_{dl}$  and  $\alpha$ ) were fitted.

## Results and Discussion

**Aspects of this work in the context of literature.**—Previous studies have shown impedance analyses conducted with changing ratios of  $R_{ct}/R_{ion}$ , most prominently done by Ogihara et al.,<sup>8–11</sup> who built a baseline theory for porous electrode impedance analysis. Their analysis is based on a simplification for the low-frequency impedance that, as we will show here, is only valid for larger values of  $R_{ct}/R_{ion}$ , a fact that is not specified in any of their publications. While these publications study a large range of  $R_{ct}/R_{ion}$ , the experimental and simulated spectra analysis stops short of reaching transport limited impedances and are thus in a range where the error made from their simplifications are still lowsmall. This is due to the fact that their studies are concerned exclusively with the impedance response of cathode electrodes, which for practical areal capacities still have high  $R_{ct}/R_{ion}$  values. On the other hand, as will be shown in the following, this is not true for graphite electrodes, which at

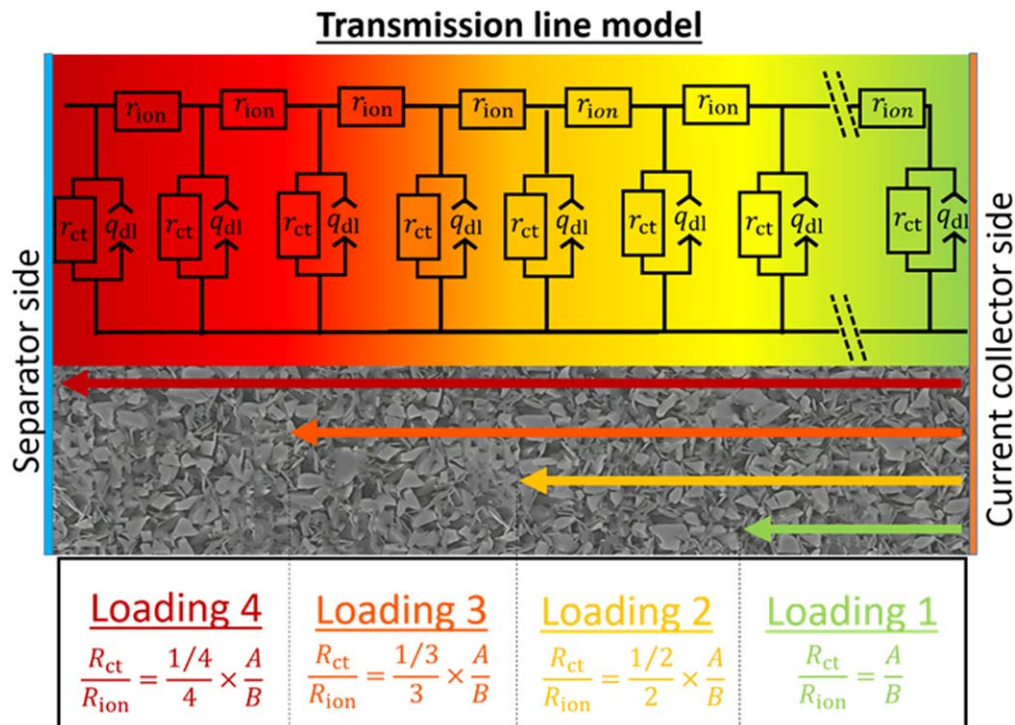


**Figure 1.** Middle panel: schematic representation of a porous LIB electrode, extending between the separator/electrode interface (left) and the electrode/current collector interface (right). Top panel: simplified transmission line model (TLM) equivalent circuit with pore resistance element  $r_{ion}$ , charge transfer resistance element  $r_{ct}$ , and capacitive elements  $q_{dl}$ , whereby  $\sum r_{ion} = R_{ion}$ ,  $\sum 1/r_{ct} = 1/R_{ct}$ , and  $\sum q_{dl} = Q_{dl}$ . Bottom panel: Influence of loading changes on the ionic resistance  $R_{ion}$  and the charge transfer resistance  $R_{ct}$ . Starting at an arbitrary active material loading where  $R_{ct}$  takes the value A and  $R_{ion}$  takes the value B, so that  $R_{ct}/R_{ion} = A/B$  (“Loading 1”), a 2-fold increase of the loading (i.e., of the areal capacity) increases the pore resistance by a factor of 2 due to the increase in electrode thickness (assuming constant porosity and tortuosity) and decreases the charge transfer resistance by a factor of 2 due to the increased electrochemically active surface area, resulting in a 4-fold lower  $R_{ct}/R_{ion}$  value (“Loading 2”). Increasing the loading by 3- or 4-fold, changes the resistances and  $R_{ct}/R_{ion}$  accordingly.

practical areal capacities have  $R_{ct}/R_{ion}$  values of  $\ll 1$ . To the best of our knowledge, we therefore show for the first time how to analyze and understand porous electrode impedance spectra over the full range of  $R_{ct}/R_{ion}$ , (from  $\gg 1$  to  $\ll 1$ ).

**Simulated and experimental impedances of porous electrodes.**—This subsection discusses the mathematical background of the transmission line model shown in Fig. 1 and examines the simulated electrode impedance spectra for different fictitious areal capacities. The simulated spectra are then compared to experimentally obtained impedance spectra of graphite anodes (acquired using a micro-reference electrode) of various areal capacities (see Table I). A subsequent analysis of the simulated current distribution vs fictitious areal capacity in the following subsection will give insights into the possible ramifications of increasing areal capacities for the charging/discharging behavior of LIB electrodes.

The equivalent circuit model shown in Fig. 1 is represented mathematically by the following equation (see Refs. 15, 16 for the general derivation)):

$$\mathbf{Z} = \sqrt{\frac{R_{ion}}{\left( (j\omega)^{\alpha} Q_{dl} + \frac{1}{R_{ct}} \right)}} \coth \left( \sqrt{R_{ion} \left( (j\omega)^{\alpha} Q_{dl} + \frac{1}{R_{ct}} \right)} \right) \quad [1]$$

where  $\mathbf{Z}$  [ $\Omega$ ] is the complex impedance of the electrode,  $\omega$  [rad/s] is the radial frequency,  $R_{ct}$  [ $\Omega$ ] and  $R_{ion}$  [ $\Omega$ ] are the charge transfer resistance of the entire electrode, and  $j$  is the imaginary unit. Furthermore, the ideal double layer capacitor element ( $C_{dl}$ ) is replaced in Eq. 1 by a constant phase element, defined as  $(j\omega)^{\alpha} Q_{dl}$  with  $\alpha$  ( $0 < \alpha \leq 1$ ). The impedance given by Eq. 1 neglects the electronic resistance of the solid phase (usually negligible for practical electrodes),<sup>2,17</sup> the diffusion phenomena of electroactive species in both electrolyte and electrode (usually appearing at very low frequencies), and the ionic resistance of the electrolyte in the separator. As Eq. 1 represents the porous electrode only (as the separator resistance is not included), its limiting case for infinitely high frequencies is  $\mathbf{Z} = 0$  (also clear from Eq. 1 that as  $\omega \rightarrow \infty$ ,

**Table I. Properties of the various here used graphite electrodes with different areal capacities by varying the graphite mass loading. The accuracy of the thickness measurement is  $\pm 3 \mu\text{m}$  (Lifematic VL-50, Mitutoyo, Japan), and the here listed electrode coating thicknesses were obtained by subtracting the thickness of the current collector. Porosities were determined by dividing the theoretical bulk volume of the graphite and PVDF components (using bulk densities of  $2.26 \text{ g cm}^{-3}$  and  $1.77 \text{ g cm}^{-3}$ , respectively) by the total electrode volume determined by the measured electrode thickness.**

Areal Capacity [ $\text{mAh cm}^{-2}$ ]	Graphite Mass Loading [ $\text{mg}_G \text{ cm}^{-2}$ ]	Thickness [ $\mu\text{m}$ ]	Porosity [%]
7.5	21.5	165	42
2.9	8.2	65	43
1.5	4.3	36	46
0.6	1.7	14	46

$Z \rightarrow 0$ ). For the low-frequency resistance, i.e., as  $\omega \rightarrow 0$ , Eq. 1 simplifies to:

$$L \equiv Z_{\omega \rightarrow 0} = \sqrt{R_{\text{ion}} \cdot R_{\text{ct}}} \coth(\sqrt{R_{\text{ion}}/R_{\text{ct}}}) \quad [2]$$

This equation represents the low-frequency resistance ( $L$  [ $\Omega$ ]) that would be obtained from an impedance measurement for a porous electrode, not taking into account the separator or the solid or liquid diffusion Warburg resistance. Next, we define  $\vartheta \equiv R_{\text{ct}}/R_{\text{ion}}$  in order to simplify Eq. 2 as follows:

$$\frac{L}{R_{\text{ion}}} = \sqrt{\vartheta} \coth(1/\sqrt{\vartheta}) \quad [2a]$$

In the following, we will describe the limiting cases, when either the charge transfer resistance ( $R_{\text{ct}}$ ) dominates the impedance response, further on referred to as *kinetically limited*, or when the ionic resistance ( $R_{\text{ion}}$ ) in the electrolyte phase within the electrode pores dominates the impedance response, further on referred to as *transport limited*. The former occurs for  $R_{\text{ion}} \ll R_{\text{ct}}$ , in which case the term  $\sqrt{R_{\text{ion}}/R_{\text{ct}}}$  in the coth function in Eq. 2 becomes very small, so that the coth function can be approximated by:

$$\lim_{y \rightarrow 0} \coth(y) = \frac{1}{y} + \frac{y}{3} + \text{higher order terms} \quad [3]$$

Simplifying Eq. 2 by this approximation of the coth function (neglecting the higher order terms), the kinetically limited value of the low-frequency electrode impedance ( $L|_{(R_{\text{ion}} \ll R_{\text{ct}})}$ ) becomes:

$$L|_{(R_{\text{ion}} \ll R_{\text{ct}})} = R_{\text{ct}} + \frac{R_{\text{ion}}}{3} \quad [4]$$

Similar to Eqs. 2a, 4 can also be expressed in terms of  $\vartheta \equiv R_{\text{ct}}/R_{\text{ion}}$  as follows:

$$\frac{L}{R_{\text{ion}}} \Big|_{(R_{\text{ion}} \ll R_{\text{ct}})} = \vartheta + \frac{1}{3} \quad [4a]$$

On the other hand, in the transport limited regime, where  $R_{\text{ion}} \gg R_{\text{ct}}$ , the term  $\sqrt{R_{\text{ion}}/R_{\text{ct}}}$  in the coth function in Eq. 2 becomes very large, so that the coth function approaches 1 (i.e.,  $\lim_{y \rightarrow \infty} \coth(y) \rightarrow 1$ ) and Eq. 2 simplifies to the expression for the transport limited low-frequency impedance ( $L|_{(R_{\text{ion}} \gg R_{\text{ct}})}$ , also see Refs. 3, 15 for derivation):

$$L|_{(R_{\text{ion}} \gg R_{\text{ct}})} = \sqrt{R_{\text{ion}} R_{\text{ct}}} \quad [5]$$

Expressing Eq. 5 via the  $\vartheta$  variable leads to the following equation:

$$\frac{L}{R_{\text{ion}}} \Big|_{(R_{\text{ion}} \gg R_{\text{ct}})} = \sqrt{\vartheta} \quad [5a]$$

In summary, in the kinetically limited regime ( $R_{\text{ion}} \ll R_{\text{ct}}$ ), Eq. 4 shows that  $R_{\text{ct}}$  constitutes the major fraction of the low-frequency resistance, so that the low-frequency resistance is a reasonably close measure of  $R_{\text{ct}}$ . On the other hand, in the transport limited regime ( $R_{\text{ion}} \gg R_{\text{ct}}$ ), Eq. 5 shows that  $R_{\text{ct}}$  cannot be evaluated directly from the low-frequency resistance.

Figures 2a and 2b show the simulated impedance spectra of electrodes for which the effect of varying active material loadings was simulated by varying  $R_{\text{ion}}$  and  $R_{\text{ct}}$ . As outlined in the discussion of Fig. 1 and as shown in the bottom panel of Fig. 1, it was assumed that a doubling of the active material loading and thus of the areal capacity would result in a halving of the charge transfer resistance (i.e.,  $R_{\text{ct}} \propto 1/C_{\text{areal}}$ ) and in a doubling of the ionic resistance (i.e.,

$R_{\text{ion}} \propto C_{\text{areal}}$ ). Thus, the simulated  $R_{\text{ct}}$  values that are decreasing from 16 to 0.5  $\Omega$  (in steps of factors of 2) represent an increase in the simulated active material loading (or areal capacity) by an overall factor of 32; this is accompanied by a 32-fold increase of  $R_{\text{ion}}$  from 1 to 32  $\Omega$  (also in steps of factors of 2). Since the double layer capacitance is expected to increase with the active material loading (or areal capacity), the  $Q_{\text{dl}}$  value was scaled from an initial value of 0.25 mF for the lowest loading (represented by  $R_{\text{ct}} = 16 \Omega$  and  $R_{\text{ion}} = 1 \Omega$ ) by  $0.25 \text{ mF} \times \frac{R_{\text{ion}}}{1 \Omega}$  for higher loadings (assuming that  $Q_{\text{dl}} \propto C_{\text{areal}}$  and that  $\alpha = 1$ ). As will be shown later, the here chosen values for  $R_{\text{ct}}$ ,  $R_{\text{ion}}$ , and  $Q_{\text{dl}}$  fall within the range of those obtained for graphite anodes with areal capacities of 0.6–7.5 mAh cm<sup>-2</sup> (see Table III).

As an idealized reference case, we start our discussion of the simulated impedance spectra for a hypothetical electrode with a low active material loading that does not have any pore resistance (i.e.,  $R_{\text{ct}} = 16 \Omega$  and  $R_{\text{ion}} = 0 \Omega$ , with  $Q_{\text{dl}} = 0.25 \text{ mF}$ ). In this case, the simulated impedance spectrum only consists of a semicircle, represented by the dashed red line in Fig. 2a. Adding a 1  $\Omega$  ionic resistance (i.e.,  $R_{\text{ct}} = 16 \Omega$  and  $R_{\text{ion}} = 1 \Omega$ ) barely changes the spectrum (orange line), except for the appearance of a short 45°-line region at high frequencies that represents the ionic resistance in the electrode pores (clearly visible in Fig. 2b). The 45°-line extends from  $\text{Re}(Z) = 0 \Omega$  until  $\sim 0.33 \Omega$ , corresponding to  $1/3 R_{\text{ion}}$ , followed at lower frequencies by a semicircle with a diameter of 16  $\Omega$ , summing up to an overall low-frequency resistance of  $L = 16.33 \Omega$ , as predicted by Eq. 4. A spectrum exhibiting such clear features allows the user to directly extract the numerical values of both  $R_{\text{ct}}$  and  $R_{\text{ion}}$  from the spectrum, as both components are represented by unique features (viz., by the diameter of the semicircle and by the real axis extension of the 45°-line, respectively).

In order to simulate the increase of the active material loading by a factor of 2, the ionic resistance is being doubled (from 1 to 2  $\Omega$ ) and the charge transfer resistance is being halved (from 16 to 8  $\Omega$ ). The simulated impedance spectrum then shows a low-frequency resistance of 8.66  $\Omega$ , but still exhibits a clear 45°-line feature with an extension along the real axis of  $R_{\text{ion}}/3 (= 2/3 \Omega)$  as well as a pronounced semicircle with a diameter corresponding to  $R_{\text{ct}}$  (8  $\Omega$ ; see yellow lines in Figs. 2a and 2b). A further simulated doubling of the active material loading by further increasing  $R_{\text{ion}}$  to 4  $\Omega$  and decreasing  $R_{\text{ct}}$  to 4  $\Omega$ , yields a low-frequency resistance of 5.33  $\Omega$  (green line) that is still well described by Eq. 4, even though  $R_{\text{ct}}/R_{\text{ion}}$  is now 1/1. Deviations from Eq. 4 are observed upon a further two-fold increase of the simulated active material loading (represented by  $R_{\text{ct}} = 2 \Omega$  and  $R_{\text{ion}} = 8 \Omega$ ; blue line), for which the simulated low-frequency resistance of 4.15  $\Omega$  (based on Eq. 1) differs from the 4.0  $\Omega$  predicted by Eq. 4 (kinetically limited regime) as well as from the 4.0  $\Omega$  predicted by Eq. 5 (transport limited regime). Hence, the electrode impedance response lies in the transition zone between the two limiting cases, and retrieving the values of  $R_{\text{ct}}$  and  $R_{\text{ion}}$  requires a more complex analysis, as described later in this publication.

Further increasing the simulated loading yields a, on the first glance, surprising result. The impedance spectra for higher simulated loadings (here  $R_{\text{ct}}/R_{\text{ion}}$  with 1/16 and 0.5/32, see dark purple line and light purple square symbols) not only have the same low-frequency resistance and fully overlap, but are also very similar to that obtained for  $R_{\text{ct}}/R_{\text{ion}} = 2/8$  (blue line). This can be understood when looking at Eq. 5 that describes the transport limited regime, where a doubling of  $R_{\text{ion}}$  and a halving of  $R_{\text{ct}}$  simulates a doubling of the active material loading and results in the identical low-frequency resistance. Thus, in the transport limited regime, the impedance spectrum does not anymore provide any information on the individual values of  $R_{\text{ion}}$  and  $R_{\text{ct}}$ , as any combination of these two resistances will yield the same low-frequency resistance and, as a matter of fact, exhibit the practically identical impedance spectrum in a Nyquist plot. To determine  $R_{\text{ion}}$  and  $R_{\text{ct}}$  from an impedance

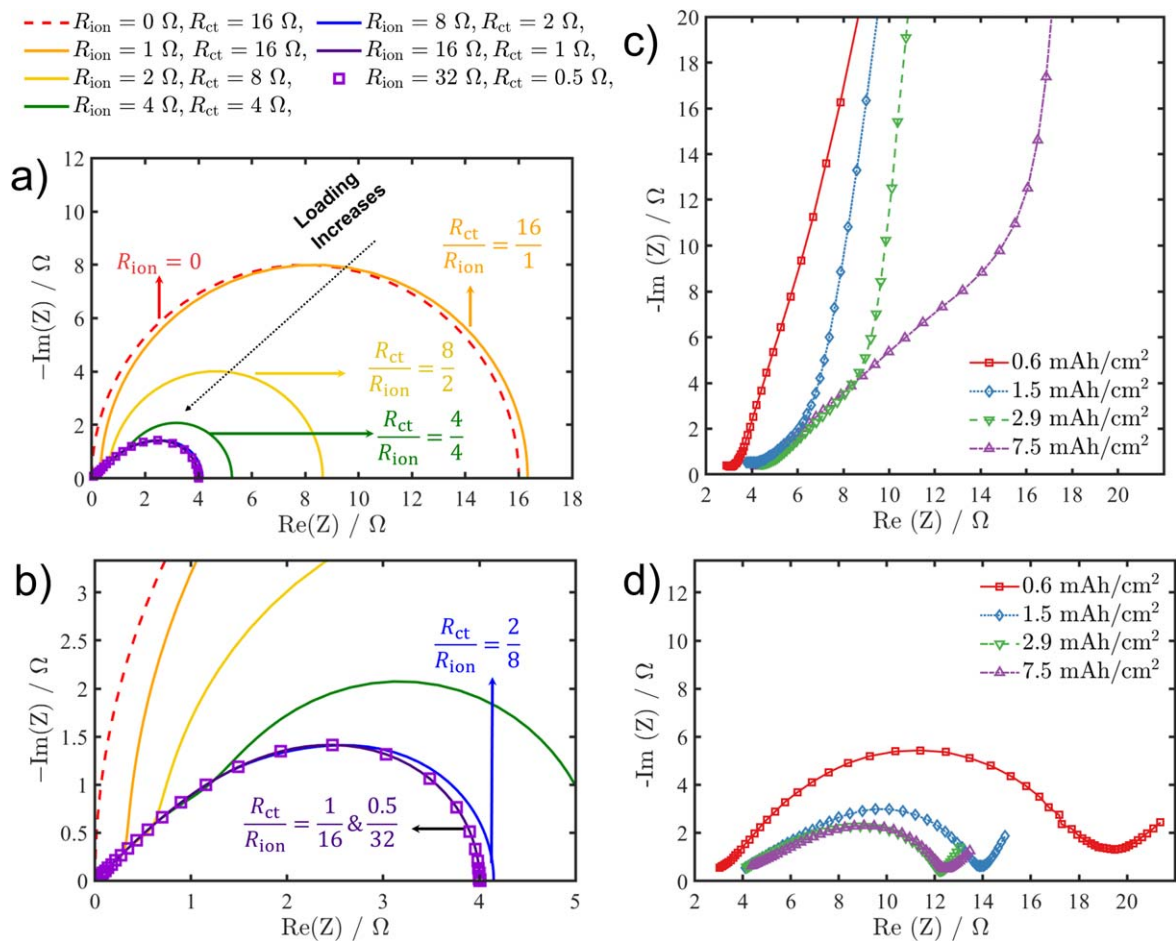


**Figure 2.** Electrode impedance spectra simulated acc. to Eq. 1 and measured for graphite anodes with different areal capacities. (a) Simulated electrode impedance spectra (Eq. 1). Parameters  $Q_{dl} = 0.25$  mF with  $\alpha$  for the constant phase element set to 1; Spectra are simulated for the frequency range of 100 kHz to 0.1 Hz. (b) Zoom into the high-frequency region of panel a. For decreasing  $R_{ct}/R_{ion}$  ratios (higher active material loadings), the distinct features of the 45°-line and the semicircle disappear and the spectrum merges into a single feature. (c) Experimentally obtained impedance spectra of graphite electrodes (measured via micro-reference electrode) with different areal capacities, recorded at 2 V vs  $Li^+/Li$  before formation (i.e., under blocking conditions). (d) Impedance spectra of the graphite electrodes at 50% SOC after two formation cycles, showing first a decrease in the low-frequency resistance (from 0.6 to 2.9  $mAh\ cm^{-2}$ ) and then a constant low-frequency resistance for 2.9 and 7.5  $mAh\ cm^{-2}$ . The graphite anode impedance data between 30 kHz and 0.1 Hz were obtained by using a micro-reference electrode. The semicircle apex frequency for the experimental data is between 110 Hz (0.6 and 1.5  $mAh\ cm^{-2}$ ) and 139 Hz (2.9 and 7.5  $mAh\ cm^{-2}$ ).

spectrum in this regime, either one of these two resistances needs to be known or to be determined independently. For example,  $R_{ion}$  could be simply acquired via measurements in blocking conditions (i.e., conditions where no faradaic reaction is possible).<sup>8,18-21</sup> A more detailed description of how to analyze impedance spectra in the transport limited regime will be shown later on.

To understand whether the impedance spectra of practical Li-ion battery electrodes fall into the kinetically or transport limited regime, we measured impedance spectra of graphite anodes with different active material loadings, i.e., with areal capacities ranging from 0.6–7.5  $mAh\ cm^{-2}$  (see Table I). Impedance spectra were acquired both before formation at 2 V vs  $Li^+/Li$ , corresponding to 0% SOC (representing blocking conditions, due to the very high  $R_{ct}$  of a pristine graphite electrode at this potential), as well as after two formation cycles and a partial charge to 50% SOC, as shown in Figs. 2c and 2d, respectively. The spectra of the pristine graphite electrodes acquired at 2 V vs  $Li^+/Li$  (= 0% SOC) exhibit the 45°-line feature (see Fig. 2c), as expected for blocking conditions,<sup>8,18,19</sup> in which case the extension of the 45°-line along the real axis corresponds to  $R_{ion}/3$  (this will be further discussed in the context of Fig. 4a). Thus, a preliminary inspection of Fig. 2c shows that  $R_{ion}$  clearly increases with increasing areal capacity (i.e., with active material loading and electrode thickness), which was the basis for our interpretation of the simulated impedance spectra

(Figs. 2a and 2b). A quantitative analysis of our assumed relationship of  $R_{ion} \propto C_{areal}$  will follow towards the end of this work.

The spectra in Fig. 2d show the graphite electrode impedances at 50% SOC after formation. The graphite electrode with the lowest areal capacity of 0.6  $mAh\ cm^{-2}$  (red line/squares) exhibits a negligible ionic resistance, as indicated by the very short 45°-line at high frequencies, but shows a large kinetic resistance, as indicated by the large diameter of the semicircle that follows at lower frequencies. This impedance spectrum is qualitatively very similar to the simulated impedance spectra for  $R_{ct}/R_{ion}$  ratios of 16/1 and 8/2 (orange and yellow lines in Figs. 2a and 2b), except that the semicircle of the experimental spectrum is somewhat suppressed, indicating a lower  $\alpha$  value (note that  $\alpha = 1$  was used for the simulated spectra). Upon increasing the areal capacity of the graphite electrode to 1.5  $mAh\ cm^{-2}$  (blue line/diamonds in Fig. 2d), the electrode resistance is reduced substantially and the impedance spectrum exhibits a now continuous transition from a high-frequency  $\sim 45^\circ$ -line feature to a suppressed semicircle feature. The experimental spectrum thus resembles the simulated spectra with  $R_{ct}/R_{ion}$  ratios somewhere in between 4/4 and 2/8 (green and blue lines in Figs. 2a and 2b). Finally, increasing the areal capacity of the graphite electrodes to 2.9 and 7.5  $mAh\ cm^{-2}$  (green line/inverted-triangles and purple line/triangles in Fig. 2d), essentially identical impedance spectra are obtained, with an electrode resistance that is only

marginally smaller than that for the  $1.5 \text{ mAh cm}^{-2}$  electrode. Furthermore, the impedance spectra of the  $2.9$  and  $7.5 \text{ mAh cm}^{-2}$  graphite electrodes resemble the spectra simulated for  $R_{ct}/R_{ion}$  ratios somewhere in between  $2/8$  and  $1/16$  (blue and purple lines in Figs. 2a and 2b), indicating that their impedance response represents the transport limited regime. The  $0.6 \text{ mAh cm}^{-2}$  electrode also shows that the assumption of the simplified TLM with one kinetic  $R/C$  element is valid, as the sample shows only one semi-circle feature associated with the kinetics. It cannot be determined from these measurements whether this spectral feature also contains contributions from the solid electrolyte interphase (SEI) formed during the first charge of the anodes, as the SEI is generally also associated with a semi-circle feature.<sup>22</sup> This, however, should not influence the impedance analysis outlined in this publication.

In summary, upon increasing the areal capacity (i.e., the active material loading) of graphite electrodes, their low frequency electrode resistance does not significantly decrease for areal capacities above  $1.5 \text{ mAh cm}^{-2}$ , suggesting a compensation of the decreasing  $R_{ct}$  by the increasing  $R_{ion}$  as the areal capacity being increased, consistent with Eq. 5 that describes the transport limited regime of the electrode impedance. Prior to presenting a methodology by which  $R_{ct}$  can be obtained even under these conditions, we will first examine the current distribution at frequencies close to where the low-frequency resistance is being determined and will show the changing sampling depth into a porous electrode at that frequency.

**Current distribution across an electrode in the  $R_{ct}$  and  $R_{ion}$  dominated domain.**—The ratio of  $R_{ct}/R_{ion}$  strongly affects the way the current distributes over the electrode. Figure 3a shows the current density distribution for a given applied current, normalized to its maximum local value at the separator/electrode interface for electrodes with different  $R_{ct}/R_{ion}$  ratios. The expression for the normalized complex current density along with its associated equivalent circuit is shown in the Appendix (see Fig. A.1 and Eq. A.9) and it is valid only under the condition that  $R_{ct}$  and  $R_{ion}$  are dominating the current response, i.e., only within the frequency range where the double layer capacitance effect has become negligible (in this case below  $\sim 10^1$  Hz) and where the diffusion in the solid and electrolyte phase is not yet significant (here above  $\sim 10^0$  Hz). Practically, Eq. 9 and Fig. 3a describe the scaled complex current density distribution in the vicinity of the imaginary impedance minimum after the (suppressed) semicircle of the spectrum

of an electrode, i.e., near the point that marks the low-frequency resistance; based on the impedance data of the graphite electrodes shown in Fig. 2d, this occurs in the vicinity of  $\sim 1$  Hz. This current distribution can thus be understood as the charging/discharging current toward the end of a short (on the order of  $10^0$  s) current pulse applied to the electrode and it is independent of the absolute current magnitude (provided that we are in the linear range of Butler-Volmer kinetics). Thus, this scaled current distribution across the electrode only depends on the  $R_{ct}/R_{ion}$  ratio and would be essentially identical for a  $C/10$  or a  $1C$  current pulse, so that it should closely reflect the current distribution after a short DCIR (direct current internal resistance) pulse, which is a commonly used diagnostic tool in Li-ion battery research.<sup>23,24</sup>

For a dominating  $R_{ct}$ , the current density distribution is mostly homogeneous throughout the electrode (lines in the red/orange shaded region, Fig. 3a). In such an electrode, the charge transfer reaction takes place (mostly) homogeneously throughout the electrode, and the active material particles would be charged or discharged uniformly across the electrode. Increasing  $R_{ion}$ , i.e., decreasing  $\vartheta$ , leads to significantly lower currents towards the electrode/separators interface (i.e., near  $x = 1$ ) and results in a less homogeneous current density distribution (green/blue shaded regions). In this case, active material particles at/near the separator/electrode interface (left side in Figs. 3a and 3b) are charged/discharged more extensively than particles at/near the electrode/CC interface. Ultimately, upon further decreasing  $\vartheta$  (purple shaded region), the current distribution becomes so skewed that parts of the electrode are practically not participating in the reaction anymore during the impedance measurement (in the frequency range on the order of  $\sim 10^0$  Hz). In such a case, the impedance response of the electrode is in the transport limited regime, and active material particles at/near the electrode/CC interface are not charged/discharged during the measurement.

The latter aspect is further illustrated in Fig. 3b, where the current distribution across electrodes with three different active material loadings (viz.,  $\delta_1$ ,  $\delta_2 = 2 \cdot \delta_1$ , and  $\delta_3 = 3 \cdot \delta_1$ ) and thicknesses is being examined, whereby the  $x$ -axis represents the electrode thickness at which a given loading is reached. For the lowest loaded electrode ( $\delta_1$ ), an  $R_{ct}/R_{ion}$  ratio of  $1/16$  was assumed, that according to Figs. 2a/2b and Fig. 3a falls within the transport limited regime. Consequently, the current density at the electrode/CC interface (at  $\delta_1$ ) is essentially zero (red circles in Fig. 3b). Increasing the loading by a factor of 2 to  $\delta_2$  and reducing  $R_{ct}/R_{ion}$  to  $0.5/32$  (blue

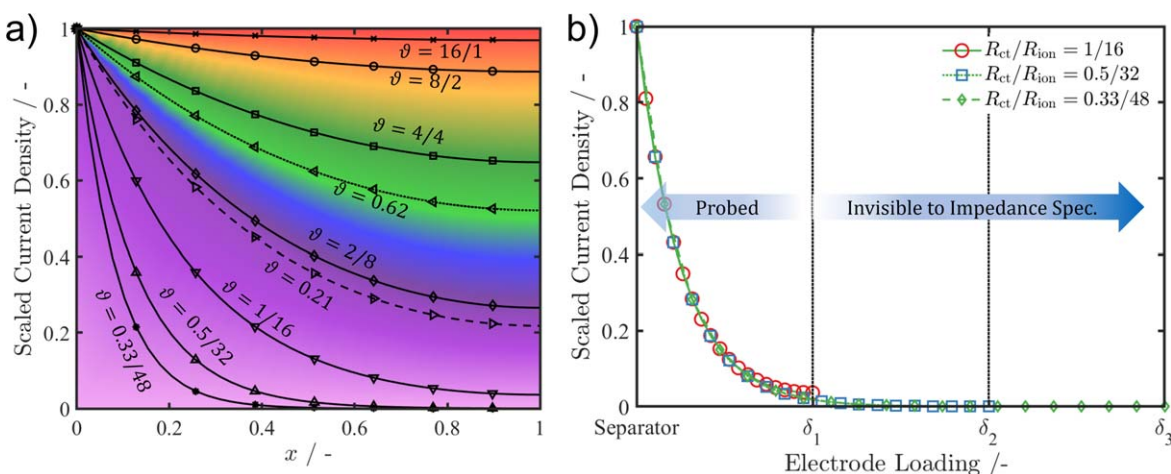


**Figure 3.** Ionic current density distribution across an electrode (scaled to the maximum current density at the separator/electrode interface) based on Eq. A.9 in the Appendix. (a) Scaled current density for different ratios of  $\vartheta = R_{ct}/R_{ion}$  vs. the normalized electrode thickness  $x$ , with  $x = 0$  being the separator/electrode interface and  $x = 1$  being the electrode/CC interface. (b) Scaled current density distribution for conceptual electrodes with three different active material loadings (and thicknesses). For the lowest loading electrode ( $\delta_1$ ), an  $R_{ct}/R_{ion}$  value of  $1/16$  was chosen, representing a transport limited electrode, and the scaled current distribution between the separator/electrode and the electrode/CC interface is shown by the red circles. For a 2-fold and 3-fold higher electrode loading and a concomitant reduction of  $R_{ct}/R_{ion}$ , the essentially identical current profile is obtained (blue squares).

squares), or by factor of 3 to  $\delta_3$  and reducing  $R_{ct}/R_{ion}$  to 0.33/48 (green diamonds), does not significantly change the current distribution anymore, as the current has already dropped to a negligible value at the electrode/CC interface even for the lowest loading (point marked  $\delta_1$ ), and since the current distributions for all three loadings are therefore overlapping. Hence, the additionally added active material mass for the loadings  $\delta_2$  and  $\delta_3$  is not visible to the impedance measurement. For a real battery (as opposed to the simplified representation shown in Fig. 1), the additional loading will be visible at very low frequencies (on the order of mHz), where the electrode will again exhibit a capacitor-like behavior due to the limited Li storage capacity in the particles.

These insights are important to consider when analyzing aged electrodes via impedance spectroscopy, since aged electrodes may have high ionic resistances due to pore blocking by SEI (solid electrolyte interphase) products and may exhibit an increased ionic resistance near the separator/electrode interface (produced, e.g., by lithium plating at the separator/electrode interface caused by fast-charging).<sup>25</sup> In these cases, only the part of the electrode near the separator/electrode interface may be probed by impedance measurements. This could lead to an incorrect interpretation of the impedance spectra, as the measured resistance would only be representative for the region of the electrode near the separator/electrode interface. It is also noteworthy that the  $R_{ct}/R_{ion}$  ratio of 1:1 ( $\vartheta = 4/4$  in Fig. 3a) is still described as kinetically limited rather than being in the transition zone between the kinetically and the transport limited regimes. This is because the kinetic resistances are connected in parallel (see Figs. 1 and A-1), i.e., all current must eventually pass through a kinetic resistive element so that the contribution of  $R_{ct}$  is larger compared to that of  $R_{ion}$ , as not all current passes through the entire ionic resistance of the electrode. This is most clearly seen in Eq. 4 where the ionic contribution is 1/3 of the total ionic resistance and the kinetic resistance is represented in full.

While the terminology of kinetically or transport limited behavior of an electrode is directly applicable for reactions that are at steady-state (as, e.g., applies to the half-cell reactions in fuel cells or electrolyzers), in which case the electrode utilization attains a steady-state value (i.e., a constant overpotential for an applied current), this terminology is more complicated in the case of battery electrodes. Intercalation reactions in finite sized particles are transient processes (no steady-state), where not all particles may participate in the reaction at the same time and where the liquid electrolyte may continuously change its concentration profile (leading to changing overpotentials) throughout the charging/discharging process. While the measured  $R_{ion}$  value is only a function of the electrolyte conductivity and the electrode pore structure, the total electrolyte overpotential during an applied current is also a function of the additional Warburg element<sup>26</sup> that incorporates diffusion coefficient, thermodynamic factor, and transference number, all of which may vary greatly between different electrolyte compositions and temperatures.<sup>27</sup> In addition, the charge transfer resistance is also a function of the lithium concentration in the electrolyte as well as in the solid phase of the active material, further complicating the analysis. Nevertheless, some fundamental statements can be made.

An important factor (other than the ratio of  $R_{ct}/R_{ion}$ ) in determining the homogeneity in lithiation/delithiation of the active material particles in an electrode for Li-ion batteries is the open circuit voltage (OCV) profile of the active material. Very steep OCV profiles, i.e., spanning over a wide potential range (e.g., NMC materials that span an OCV range of  $\sim 1.1$  V within their operating window, viz., from  $\sim 3.3$ - $4.4$  V vs  $\text{Li}^+/\text{Li}$ ) generally charge more homogeneously compared to active materials that charge/discharge over a narrow OCV range, especially if the overpotential is small compared to the OCV window. For the former materials, the thermodynamic potential (i.e., the OCV) becomes the deciding factor in determining the particle SOC. On the other hand, for active materials with a narrow OCV range (e.g., graphite with its two

main lithiation stages,  $\text{Li}_4\text{Ti}_5\text{O}_{12}$  (LTO), or  $\text{LiFePO}_4$  (LFP)), the degree of lithiation of the electrode is only weakly dependent on the electrode OCV. In such cases of narrow OCV ranges, the  $R_{ct}/R_{ion}$  ratio can be a deciding factor determining the current distribution, even for longer current applications, resulting in a current “front” moving from the separator interface to the current collector interface for severely transport limited electrodes. Other factors like the active material particle size distribution also need to be considered. As small particles would generally lithiate faster, the current distribution of a transport limited electrode would not only move from the separator to the current collector interface but also from small to large particles.

**Impedance analysis guidelines for porous electrodes.**—The following subsection gives a guideline on how to determine  $R_{ct}$  and  $R_{ion}$  from the low-frequency resistance ( $L$ ) obtained from individual electrode impedance data using the TLM represented by Eq. 1 and its low-frequency solution given by Eq. 2. For this, it is important to understand whether the impedance response of a given electrode falls within the kinetically or the transport limited regime, which depends on the  $R_{ct}/R_{ion}$  ratio that in turn depends on the actual active material and electrolyte as well as on the active material loading. Since the impedance response in the transport limited regime becomes independent of the active material loading or areal capacity (see Fig. 2), a deconvolution of  $R_{ct}$  and  $R_{ion}$  in this regime requires an independent measurement of one of the two resistances (i.e., even a fit of Eq. 1 to the impedance data will practically not yield a unique solution anymore, as indicated also by Eq. 5 and discussed in a later section). The practical implications of analyzing transport limited electrode impedance spectra are detailed later on.

Table II shows the regions that we define as the kinetically or transport limited regimes. At one extreme, when  $R_{ct} \ll R_{ion}$  (i.e.,  $\vartheta \rightarrow 0$ ), the impedance response becomes transport limited and the low-frequency resistance ( $L$ ) can be described by Eqs. 5 or 5a. At the other extreme, when  $R_{ct} \gg R_{ion}$  (i.e., for  $\vartheta \rightarrow \infty$ ), the impedance spectrum can be visually separated into its transport resistance contribution and  $R_{ct}$ ; here, the low-frequency resistance is described by Eqs. 4 or 4a. Even though Eqs. 4/4a and 5/5a are only strictly correct under the limiting conditions of  $R_{ct}/R_{ion} = \vartheta \rightarrow \infty$  and  $R_{ct}/R_{ion} = \vartheta \rightarrow 0$ , respectively, they still provide a good approximation for the low-frequency resistance  $L$  over a rather wide  $R_{ct}/R_{ion}$  range. For a given low-frequency resistance  $L$  that can be determined from the impedance response of an electrode, we define the error ( $\epsilon_\vartheta \equiv |(\vartheta_{\text{true}} - \vartheta_{\text{approx}})/\vartheta_{\text{true}}|$ ) in the prediction of  $\vartheta$ , using the full solution (Eqs. 2 or 2a) vs the simplified solutions for the kinetically limited regime (Eqs. 4 or 4a) or the transport limited regime (Eqs. 5 or 5a). Tolerating 5% error in the determined  $\vartheta$  value, the range of validity of the simplified solutions is given in Table II. It shows that use of Eqs. 4/4a will only give rise to  $\leq 5\%$  error (overprediction) in the value of  $\vartheta$  compared to the full solution given by Eqs. 2/2a for  $L/R_{ion} \leq 0.46$  (corresponding to  $\vartheta \leq 0.21$ ); similarly Eqs. 5/5a will produce  $\leq 5\%$  error (underprediction) in the value of  $\vartheta$  for  $L/R_{ion} \geq 0.92$  (corresponding to  $\vartheta \geq 0.62$ ). These values give the practical boundaries which henceforth are considered to be kinetically limited ( $L/R_{ion} \geq 0.92$ ), transport limited ( $L/R_{ion} \leq 0.46$ ), or being in the transition zone.

In the following, we will describe how the value for  $R_{ct}$  can be determined from electrode impedance measurements, even if it is not known a priori whether  $R_{ct}$  or  $R_{ion}$  is dominant. The outlined procedure is expected to yield accurate results for electrodes that have not yet undergone extensive cycling; for aged electrodes, the above discussed restrictions apply. Figure 4 depicts the analysis process to determine the charge transfer resistance for porous electrodes which have an either kinetically or transport limited impedance response, or whose impedance response falls within the transition region. For each step described below, please refer to the respective step described in Fig. 4.

**Step #1: determine  $R_{ion}$ .**—In the most general case, the pore resistance stemming from the electrolyte filled pores needs to be measured under blocking conditions that can be achieved by recording the impedance spectrum either at a potential where no faradaic reaction can take place (as shown in Fig. 2c; ideally conducted prior to electrode formation) or by using an electrolyte that does not contain any reacting species (a so-called “blocking electrolyte”).<sup>19–21</sup> Such measurements can either be done using a symmetric cell setup (as shown by Landesfeind et al.<sup>19</sup>) or in a full-cell when using a micro-reference electrode to determine the impedance of each individual electrode (as done in Fig. 2c). From the thus obtained impedance spectra,  $R_{ion}$  can be extracted by taking the difference between the low- and high-frequency intercepts which equals  $R_{ion}/3$ , as illustrated in Fig. 4a (in case of symmetric cell measurements,  $R_{ion}$  of an individual electrode would then be a half of the  $R_{ion}/3$  value obtained from the cell).

**Step #2: determine  $L$ .**—The low-frequency electrode resistance  $L$  is the resistance difference between the low- and high-frequency region of the spectrum (see Fig. 4b). The value of  $L$  excludes the high-frequency contributions by the separator resistance and by electrical contact resistances (both of them are accounted for in the high-frequency intercept value). Moreover, we also assume that the diffusion processes (both in the electrolyte and in the solid phase) are slow enough that their contribution to the value of  $L$  can be neglected. An example of how to assign different phenomena to different parts of the spectra can be found in Refs. 20, 21. Additionally, the apex frequency ( $f_{apex}$ ) and the imaginary resistance  $Im_{apex}$  (taken as the modulus, since  $Im_{apex}$  is a negative number) can be evaluated by taking the frequency and imaginary resistance of the highest point of the impedance spectrum (the apex of the (suppressed) semicircle feature of the spectrum). Both values are later needed to determine the  $\alpha$  coefficient of the constant phase element that represents the double layer capacitance (see Fig. 1), as described in the subsequent sections.

**Step #3: use  $L/R_{ion}$  to classify the electrode impedance response.**—The ratio between the electrode low-frequency resistance  $L$  and the pore resistance  $R_{ion}$  marks whether the electrode impedance response is kinetically or transport limited, or whether it is in the transition region. As outlined in Table II, if  $L/R_{ion} \geq 0.92$ , the system can be treated as kinetically limited (region marked in the upper right-hand corner of Fig. 4c), and Eq. 4 can be used (see step #4a below). If the ratio  $L/R_{ion} \leq 0.46$ , the system can be considered as transport limited (region marked in the lower left-hand corner of Fig. 4c), and Eq. 5 can be used (see step #4b below). In between these two values ranges, the impedance response of the electrode falls within the transition region (gray shaded field in Fig. 4c) and the spectrum can be analysed according to step #4c below and the description of Fig. 5.

**Step #4a:  $R_{ct}$  and  $R_{ion}$  quantification in the kinetically limited regime.**—The kinetically limited regime allows for the simplest and certainly most commonly known way to analyze the impedance data of an electrode, as the features of the individual resistances are clearly discernible (see yellow, orange, and green lines in Figs. 2a/2b). In this regime, one can simply use the semicircle in the spectrum to determine the charge transfer resistance and then use the low-frequency resistance  $L$  to determine  $R_{ion}$  via Eq. 4 (the blue dashed line in Fig. 4c corresponds to Eq. 4a). Alternatively, if  $R_{ion}$  was determined from an impedance measurement under blocking conditions (see step #1),  $R_{ct}$  can be determined via Eq. 4. Note that blocking conditions constitutes a state of the electrode where  $R_{ct}$  is significantly larger than  $R_{ion}$ , and is therefore a limiting case of the kinetically limited regime.

The double layer capacitance can be determined from the apex frequency of the semicircle ( $f_{apex}$ ) using the equation provided in the

lower blue shaded field in Fig. 4c (labeled Step 4a) after determination of the  $\alpha$  coefficient of the constant phase element. To determine the latter, we refer the user to Fig. 5. Alternatively, as the spectrum in the kinetically limited regime shows a pronounced semicircle, the semicircle features can also be fitted using an  $R/Q$  element to directly get  $\alpha$  and  $Q_{dl}$ , which can be done with most impedance fitting software. Figure 4c shows the comparison between the simplified expression for the low-frequency resistance scaled by  $R_{ion}$  (Eq. 4a, blue dashed line) and the full solution (Eq. 2a, red line). Finally, it should be noted that in the kinetically limited regime, a fit of the electrode impedance data to Eq. 1 would also allow for an unambiguous quantification of  $R_{ct}$ ,  $R_{ion}$ , and  $Q_{dl}$ .<sup>9,20</sup>

**Step #4b:  $R_{ct}$  and  $R_{ion}$  quantification in the transport limited regime.**—Electrode impedance spectra representing the transport limited regime can be just as easily evaluated as those in the kinetically limited regime, just using a different set of equations. In this regime, however,  $R_{ion}$  must be determined a priori (acc. to step #1), since the low-frequency resistance  $L$  contains the product of  $R_{ion}$  and  $R_{ct}$  (Eq. 5), and since the features representing each of the two resistances cannot anymore be discerned in the spectrum (see blue and purple lines in Figs. 2a/2b). Also, the apex frequency of the spectrum can be used to determine the double layer capacitance using the same equation as for the kinetically limited regime except for an additional  $\alpha$ -dependent correction factor  $P_\alpha$ , as shown in in the lower green shaded field in Fig. 4c (labeled Step 4b) and in Fig. 5b. To determine the  $\alpha$  coefficient, we refer the user to Fig. 5a. Figure 4c shows the comparison between the simplified expression for the low-frequency resistance in the transport limited regime (Eq. 5a, green dashed curve) and the full solution (Eq. 2a, red curve).

Finally, it should be noted that in the transport limited regime a fit of the impedance spectrum to the TLM described by Eq. 1 practically cannot yield a unique solution for  $R_{ct}$  and  $R_{ion}$  anymore (see section below), so that an independent determination of  $R_{ion}$  is required (acc. to step #1).

**Step #4c:  $R_{ct}$  and  $R_{ion}$  quantification in the transition region.**—If the electrode’s impedance response is neither kinetically limited nor transport limited, the impedance analysis cannot be conducted using the simplified expressions (Eqs. 4 and 5), and the full solution (Eq. 2) must be used. One approach will be to use the full complex impedance solution (Eq. 1) to fit the experimental data to obtain  $R_{ct}$ ,  $R_{ion}$ , and  $Q_{dl}$ , but in general a unique fit requires an independent quantification of  $R_{ion}$  under blocking condition, either as described in step #1 or by driving the electrode into blocking condition during a cell cycling protocol, as shown by Landesfeind et al.<sup>20,21</sup>

Here, we aim to simplify that procedure and present a graphically based method to determine  $R_{ct}$  with in the transition region. It is in principle identical to the above described approach for the transport limited regime, except that Eq. 2a (i.e., the red line in Fig. 4c) is used to determine  $R_{ct}/R_{ion}$ : (i)  $R_{ion}$  is obtained acc. to step #1; (ii)  $R_{ct}/R_{ion}$  is obtained from the measured value of  $L/R_{ion}$  using the red solid curve in Fig. 4c (corresponding to the full solution as expressed in Eq. 2).

From the thus obtained  $R_{ct}/R_{ion}$  ratio, one can refer to Fig. 5a to determine the constant phase exponent  $\alpha$  from the measured values of the low-frequency resistance  $L$  and the modulus of the imaginary impedance at the apex frequency  $Im_{apex}$ . With  $\vartheta$  and  $\alpha$  known, the value of the scaled peak frequency ( $\hat{f}_{apex}$ ) can be obtained from Fig. 5b, from which together with the above determined values of  $R_{ct}$  and  $\alpha$  and the measured value of the apex frequency  $f_{apex}$ , the value of the double layer capacitance  $Q_{dl}$  can be determined from Eq. 6. It should be noted that Fig. 5 is generated using Eq. 1 in order to facilitate a graphical extraction of the  $\alpha$  exponent (for values of 1–0.7) and the double layer capacitance. The following definition ( $\hat{f}_{apex}$ ) can be used to calculate the double layer capacitance ( $Q_{dl}$ ).



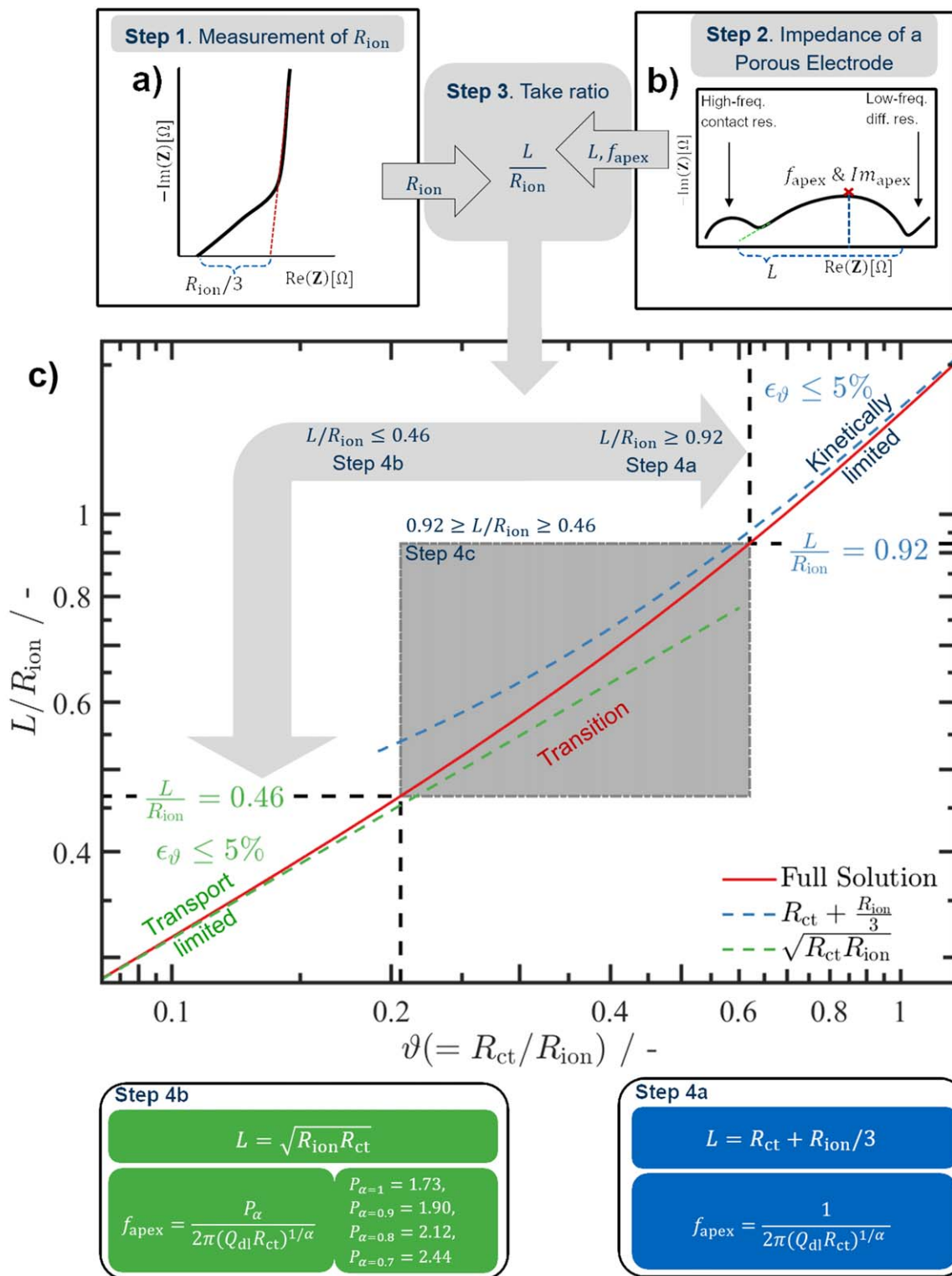


**Figure 4.** Step-by-step guidelines for the deconvolution of the charge transfer resistance ( $R_{ct}$ ) from the impedance response of a battery electrode. (a) Recording of the electrode impedance spectrum under blocking conditions, which allows the extraction of the electrode pore resistance ( $R_{ion}$ ) (b) Recording of the electrode impedance spectrum at a given SOC ( $\neq 0\%$  SOC), from which the low-frequency electrode resistance ( $L$ ) can be determined as well as the apex frequency ( $f_{apex}$  [Hz]) and the imaginary impedance at the apex frequency ( $\text{Im}_{apex}$  [ $\Omega$ ]). (c) Plot of the low-frequency resistance  $L$  normalized to the pore resistance  $R_{ion}$  vs  $R_{ct}/R_{ion} \equiv \vartheta$ , showing the precise relationship given by Eq. 2a (red line) that can be approximated in the kinetically limited regime (i.e., for  $L/R_{ion} \geq 0.92$  or  $\vartheta \geq 0.62$ ) by Eq. 4a (blue dotted line and blue shaded panel) and in the transport limited regime (i.e., for  $L/R_{ion} \leq 0.46$  or  $\vartheta \leq 0.21$ ) by Eq. 5a (green dashed line and green shaded panel).

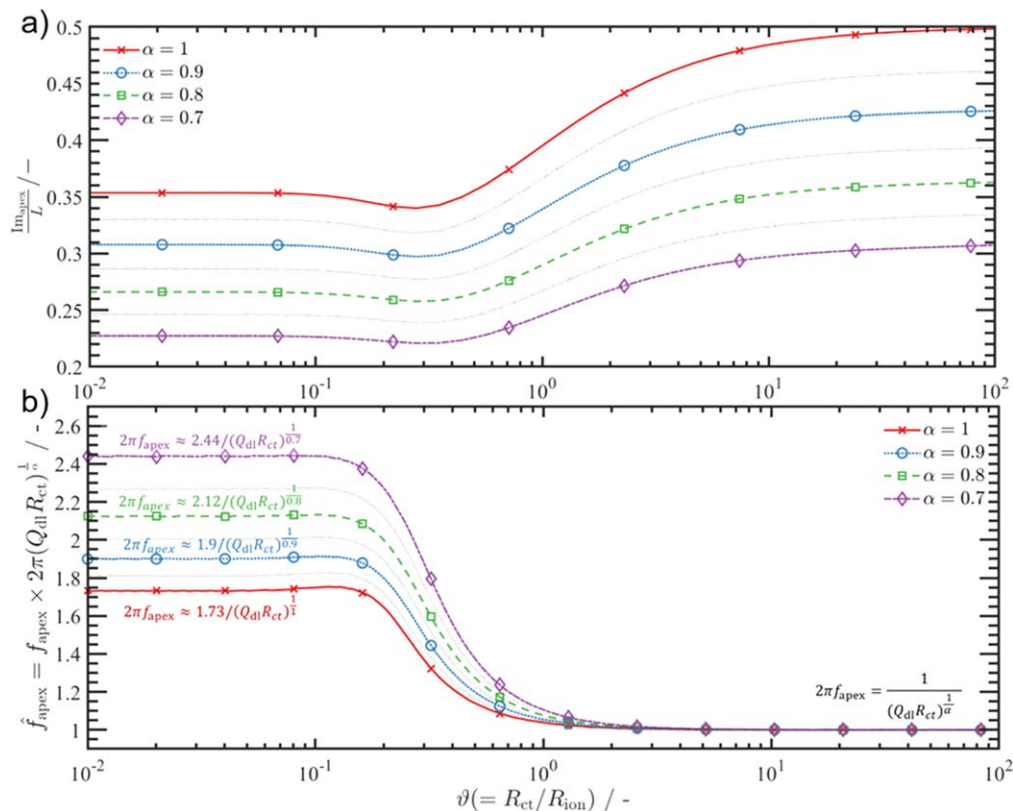


**Figure 5.** (a) Graphical representation of  $Im_{apex}/L$  vs  $\vartheta$  to allow the extraction of the constant phase element exponent  $\alpha$  between values of 1–0.7 in steps of 0.05. (b) Scaled apex frequency ( $\hat{f}_{apex}$ ) for values of the constant phase exponent  $\alpha$  from 1 to 0.7 in steps of 0.05. The graph allows to extract all information necessary to determine the electrode capacitance value  $Q_{dl}$  as described in Eq. 6.

$$\underbrace{\hat{f}_{apex}}_{\text{determined from Fig. 5b}} = \underbrace{f_{apex}}_{\text{experimentally measured}} \times 2\pi \left( \underbrace{R_{ct}}_{\text{from Fig. 4c}} \times \underbrace{Q_{dl}}_{\text{unknown}} \right)^{\frac{1}{\alpha}} \quad [6]$$

The values for  $\alpha$  are given between 1 and 0.7. Values above 1 are considered not physically viable, whereas values below 0.7 should be treated with caution, since such low  $\alpha$  values may be a result of diffusion phenomena that are not considered in Eq. 1 (a 45°-line resulting from diffusion phenomena can be described by a  $Q$  element with an exponent of  $\alpha = 0.5$ ).

**Example impedance analysis.**—The following subsection gives an example on the use of the above described method to determine  $R_{ct}$ ,  $R_{ion}$ , and  $Q_{dl}$  from the experimentally obtained impedance data for the graphite electrode with an areal capacity of a 2.9 mAh cm<sup>-2</sup>, whose impedance response under blocking and non-blocking conditions is shown in Figs. 2c and 2d, respectively. Subsequently, the analysis results are shown for all four graphite electrodes and the results are compared to the simulated impedance responses shown in Figs. 2a/2b.

Figure 6a re-plots the impedance data for a graphite electrode with an areal capacity of 2.9 mAh cm<sup>-2</sup> under blocking conditions from Fig. 2c, acquired at 2 V vs Li<sup>+</sup>/Li before formation. The procedure outlined above as Step #1 describes how to retrieve  $R_{ion}$  from the measurement by determining the difference between the projected high-frequency intercept (HFR) and the projected low-frequency intercept, as indicated by the green dashed lines. For this single dataset, this difference amounts to 9  $\Omega$  – 4.45  $\Omega$  = 4.55  $\Omega$  and corresponds to  $R_{ion}/3$ , yielding a value of  $R_{ion} = 13.7 \Omega$ . Following

Step #2, we next determine the low-frequency electrode resistance  $L$  from the impedance spectrum recorded at 50% SOC (green line in Fig. 2d, replotted in Fig. 6b), which corresponds to the difference between the projected HFR intercept and the projected low-frequency intercept, as shown in Fig. 6b. This results in  $L = 12.2 \Omega$  – 3.25  $\Omega$  = 8.95  $\Omega$ . Here, one must be careful to exclude Warburg-like diffusion phenomena arising at the low-frequency end of the spectrum. Additionally, the apex frequency value ( $f_{apex}$ ) and the modulus of the imaginary impedance at the apex frequency ( $Im_{apex}$ ) can be determined, which for this example amount to  $f_{apex} = 139$  Hz and  $Im_{apex} = 2.29 \Omega$ .

As described in Step #3, the  $L/R_{ion}$  ratio determines whether the impedance response of the electrode is in the kinetically limited, transport limited, or the in the transition regime. In case of the here examined 2.9 mAh cm<sup>-2</sup> graphite electrode,  $L/R_{ion} = 0.66$ , i.e., acc. to Table II, the impedance response of the electrode is in the transition regime, as can also be seen from Fig. 4c.

Therefore, the analysis should proceed acc. to Step #4c, determining the x-axis value of the red line in Fig. 4c that corresponds to the y-axis value of  $L/R_{ion} = 0.66$ , resulting in  $R_{ct}/R_{ion} \approx 0.37$ . Thus, based on the above value of  $R_{ion} = 13.7 \Omega$  determined under blocking conditions, the resulting  $R_{ct}$  value is 5.05  $\Omega$ . To accurately determine the capacitance of the interface, the value of the  $\alpha$  coefficient needs to be known. Usually this can be done by analyzing the blocking low-frequency spectrum via an  $R/Q$  element. Alternatively, Fig. 5a allows to determine the  $\alpha$  coefficient from the spectrum. In this case, the blocking spectrum was measured before SEI formation with an  $\alpha = 0.95$  whereas the analysis of the data at 50% SOC (assuming  $R_{ion} = 13.7 \Omega$ ) gave a value of  $\alpha = 0.78$ , meaning that the change in surface by the SEI changed the  $\alpha$  coefficient. Therefore Fig. 5 allows for the determination of  $\alpha$  from the non-blocking spectrum.

**Table II.** Overview of the applicability of the simplified Eqs. 4/4a for the kinetically limited regime and Eqs. 5/5a for the transport limited regime to predict the value of  $\vartheta \equiv R_{ct}/R_{ion}$  from the low-frequency resistance ( $L$ ) obtained from the impedance response of an electrode. The range of  $L/R_{ion}$  giving  $\leq 5\%$  error in the prediction of  $\vartheta$  shows that the expressions are valid for a much broader range of  $\vartheta$  and not just in the extremes ( $\vartheta \ll 1$  and  $\vartheta \gg 1$ ).

$\vartheta \equiv R_{ct}/R_{ion}$	kinetically limited	for any value of $\vartheta$	transport limited
applicable eqn.	$L = R_{ct} + \frac{R_{ion}}{3}$ [4]	n.a.	$L = \sqrt{R_{ion}R_{ct}}$ [5]
for L	$\frac{L}{R_{ion}} = \vartheta + \frac{1}{3}$ [4a]		$\frac{L}{R_{ion}} = \sqrt{\vartheta}$ [5a]
5% error in $\vartheta$ ( $\epsilon_{\vartheta} \leq 5\%$ )	$L/R_{ion} \geq 0.92$ $\vartheta \geq 0.62$		

For  $\vartheta = 0.37$  and  $Im_{apex}/L = 0.26$ , Fig. 5a gives  $\alpha = 0.8$ . Thus Fig. 5b gives  $\hat{f}_{apex} = 1.35$  Hz. Next, Eq. 6 will be used to get the value of  $Q_{dl}$  as shown below.

$$1.35 = 136 \text{ Hz} \times 2\pi(5.05 \times Q_{dl})^{0.78}$$

This yields a constant phase element capacitance value of  $Q_{dl} = 1.29 \text{ mFs}^{\alpha-1}$ .

Table III shows the analysis of the individual experimental data points from Figs. 2c/2d and gives a comparison to the values from a fit to Eq. 1. To fit the impedance spectra, the pore resistance is measured separately under blocking conditions prior to cycling the electrode (see Fig. 2c) and kept constant for the fitting process. This is necessary, as Eq. 5 shows that different combinations of  $R_{ct}$  and  $R_{ion}$  can give the same low-frequency impedance intercept. The fitted data are in good agreement with the manually obtained datapoints. Table III also shows the main finding of this work: if the low-frequency electrode resistance ( $L$ ) were to be interpreted as

charge-transfer resistance for the graphite electrode with an areal capacity of  $7.5 \text{ Ah cm}^{-2}$ , i.e., if one were to assume incorrectly that the experimental impedance spectrum were to represent a suppressed semicircle (contrary to our above presented analysis), one would estimate a charge transfer resistance of  $9.28 \Omega$  (entire value of  $L$ ) as opposed to the true  $R_{ct}$  value of  $\sim 2.37 \Omega$ .

To evaluate whether our initial assumptions outlined in Fig. 1 are correct, namely that  $R_{ct}$  scales inversely and that  $R_{ion}$  scales proportionally with the areal capacity, Table IV shows the experimentally determined areal capacity-scaled values for  $R_{ion}$  and  $R_{ct}$ . For all of the here examined graphite electrodes ( $0.6\text{--}7.5 \text{ mAh cm}^{-2}$ ),  $R_{ion}/C_{areal}$  is practically constant (see 3rd column of Table IV), as expected for electrodes of constant porosity (see Table I) if the tortuosity is independent of the areal capacity, i.e., of the graphite loading. The latter point can be checked by calculating the tortuosity of the electrodes via  $\tau = \frac{R_{ion} \cdot \epsilon \cdot \kappa \cdot A}{d}$ , with  $\epsilon$  being the electrode porosity,  $A$  the geometric electrode area ( $0.94 \text{ cm}^2$ ),  $\kappa$  the electrolyte conductivity ( $8.9 \text{ mS cm}^{-1}$ ), and  $d$  the electrode thickness

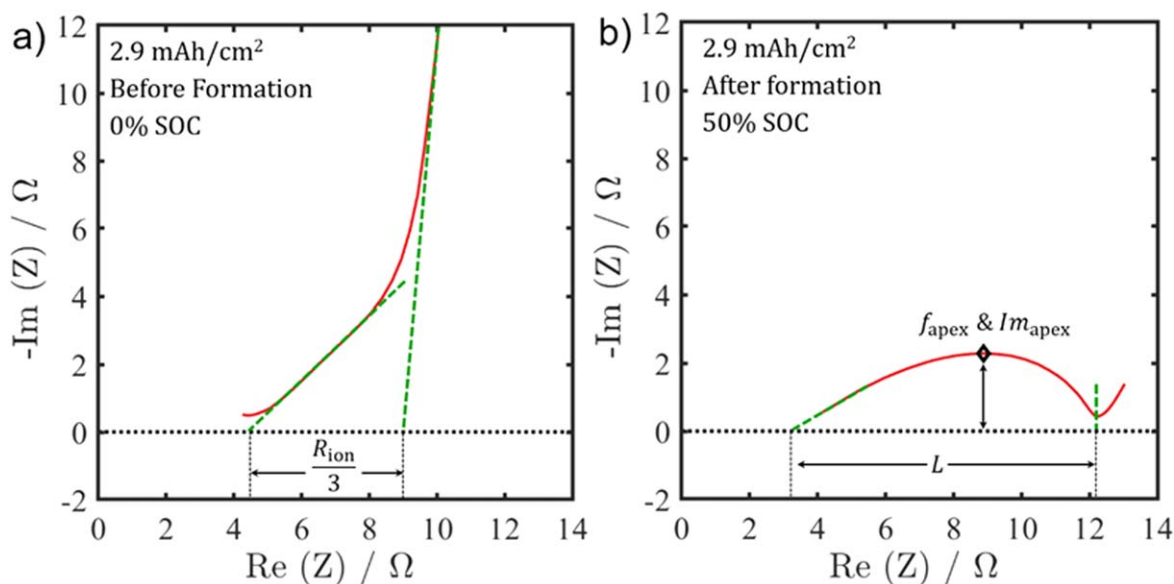


**Figure 6.** Exemplary analysis of the experimentally obtained impedance data of the graphite electrode with an areal capacity of  $2.9 \text{ mAh cm}^{-2}$  (spectra re-plotted from Figs. 2c and 2d). (a) Impedance spectrum under blocking condition, acquired at 2 V vs  $\text{Li}^+/\text{Li}$  prior to formation (data from Fig. 2c). The difference between the projected low- and high frequency intercepts (see dashed green lines) corresponds to  $R_{ion}/3$ . (b) Impedance spectrum acquired at 50% SOC after two formation cycles (data from Fig. 2d). The low-frequency electrode impedance  $L$  corresponds to the difference between the projected high- and low-frequency intercepts of the spectrum (see dashed green lines). Also  $f_{apex}$  and  $Im_{apex}$  are determined from the point of the spectrum with the highest imaginary value.

**Table III.** Parameter values determined using the method described in this publication ( $R_{ct}$ ,  $\alpha$ , and  $Q_{dl}$ ) and parameters from a spectra fit ( $R_{ct,fit}$ ,  $\alpha_{fit}$ , and  $Q_{dl,fit}$ ) for the experimental impedance data shown in Figs. 2c/2d. The data were fitted to the complex impedance solution represented by Eq. 1, keeping the  $R_{ion}$  value determined under blocking conditions prior to cycling (see Fig. 2c) constant, and then fitting the remaining variables in the impedance spectrum.

C <sub>areal</sub> [mAh/cm <sup>2</sup> ]	$R_{ion}$ [ $\Omega$ ]	$L$ [ $\Omega$ ]	$R_{ct}$ ( $R_{ct,fit}$ ) [ $\Omega$ ]	$f_{peak}$ [Hz]	$Im_{apex}$ [ $\Omega$ ]	$\alpha$ ( $\alpha_{fit}$ ) [—]	$Q_{dl}$ ( $Q_{dl,fit}$ ) [mFs <sup><math>\alpha-1</math></sup> ]
7.5	36.3	9.28	2.37 (2.27)	139	2.29	0.76 (0.74)	3.84 (5.03)
2.9	13.7	8.95	5.05 (5.01)	139	2.29	0.80 (0.78)	1.14 (1.35)
1.5	6.70	10.7	8.50 (8.70)	110	3.00	0.80 (0.74)	0.75 (0.97)
0.6	2.80	16.8	15.8 (16.2)	110	5.41	0.76 (0.74)	0.44 (0.51)

(see Table I). The thus calculated tortuosity values are indeed essentially identical ( $\tau = 7.4 \pm 0.3$ , see 4th column in Table IV), whereby the absolute tortuosity values are slightly higher than those reported previously for similar graphite electrodes ( $\tau \approx 5.0$ – $5.5$ , see Refs. 17, 19). Overall, however, the initially assumed scaling relationship of  $R_{ion}/C_{areal} = \text{constant}$  is confirmed by the experimental data.

The capacity-scaled  $R_{ct}$  (i.e.,  $R_{ct} \times C_{areal}$ ), expected to also be constant, shows an increase by a factor of  $\sim 1.8$  as the areal capacity increases by a factor of 12.5, i.e., as the graphite loading of the electrodes increases by a factor 12.5. This implies that, the experimentally determined charge transfer resistance is  $\sim 1.8$  times higher than expected based on the initially assumed scaling law of  $R_{ct} \times C_{areal} = \text{constant}$  for the highest loading. One reason for the deviation could be possible differences in the formation of a thin kinetically limited electrode and a thick transport limited electrode: A kinetically limited thin electrode is charged homogeneously during the formation cycle, and the individual active material particles all see the  $C/10$  homogeneous current throughout the formation. On the other hand, the thick electrodes are likely charged more inhomogeneously (as explained via Fig. 3), with higher local currents as the active material particles are being charged successively starting at the separator/electrode interface towards the electrode/current collector interface. This may influence the SEI formation and thus the electrode kinetics, as the active material particles are effectively undergoing formation at a higher C-rate. An alternative explanation might be related to the effect of binder migration during the drying of electrode inks, resulting in an inhomogeneous distribution of pore resistances across the electrode thickness that can cause a locally higher calculated  $R_{ct}$  (see Refs. 28, 29). A locally higher  $R_{ion}$  compared to the average  $R_{ion}$  of the electrode would lead to a greater measured electrode impedance ( $L$ ), hence leading to increased calculated (i.e., overestimated) values for the charge transfer resistance. Analyzing the phase angle of the experimental impedance spectra shown in Fig. 2 (acc. to Ref. 29, phase angle analysis not shown) suggests that this might indeed be

the case here for the 7.5 mAh cm<sup>-2</sup> electrode. This ties in with the aforementioned caution of evaluating data of aged and potentially inhomogeneous electrodes, as  $R_{ct}$  is calculated based on the assumption of a homogenous electrode via a measurement which can be distorted by inhomogeneities in the electrode.

Lastly, Table IV also shows the experimentally determined ratio of  $R_{ct}/R_{ion}$  for the different graphite electrodes, from which the impedance regime for a given electrode can be determined based on Table III or Fig. 4c. Here, only the highest loaded electrode (7.5 mAh cm<sup>-2</sup>) is fully transport limited, whereas the 2.9 mAh cm<sup>-2</sup> electrode is in the transition regime. The two lowest loaded electrodes with areal capacities of 1.5 mAh cm<sup>-2</sup> and 0.6 mAh cm<sup>-2</sup> are both kinetically limited. This shows that Li-ion battery electrodes of relevant loadings above 1.5 mAh cm<sup>-2</sup> can show significant transport resistances, visible in the invariable impedance response with increasing areal capacity shown in Fig. 2. Thus, an interpretation of the impedance spectra of graphite electrodes with practically relevant areal capacities requires a careful analysis of their transport resistance contribution to the impedance spectrum.

**Accuracy of impedance fits in the transition or transport limited regime.**—The following subsection gives an overview over the accuracy when fitting porous electrode impedance spectra (utilizing Eq. 1) using both simulated and experimental data. We compare a simulated spectrum for a given set of  $R_{ion}$ ,  $R_{ct}$ ,  $Q_{dl}$ , and  $\alpha$  that are chosen to represent the transport limited regime (i.e.,  $R_{ct}/R_{ion} < 0.21$ , see Fig. 4c) with various impedance fits conducted with different fixed values for  $R_{ion}$  (with  $R_{ct}$ ,  $Q_{dl}$ , and  $\alpha$  as fitting parameters), examining the fitting errors when fitting the simulated spectrum with incorrect  $R_{ion}$  values. This illustrates that fixed  $R_{ion}$  values that are different by factors of 2 from the actual  $R_{ion}$  value that was used to generate the simulated spectrum still yield rather small errors in the impedance fit. We then show a chosen experimental impedance spectrum from an electrode in the transition regime (i.e., the 2.9 mAh cm<sup>-2</sup> electrode, see Table IV) and give the fitting residuals calculated by fitting the experimental spectrum with

**Table IV.** Experimentally obtained electrode resistances  $R_{ion}$  and  $R_{ct}$  for graphite electrodes with different areal capacities (data from Table III), which are then used to calculate the values for  $R_{ion}/C_{areal}$ , the tortuosity ( $\tau$ ),  $R_{ion} \times C_{areal}$ , and  $R_{ct}/R_{ion}$ . The latter ratio then allows to classify the impedance response regime, based on Table II.

C <sub>areal</sub> [mAh/cm <sup>2</sup> ]	$R_{ion}$ [ $\Omega$ ]	$R_{ion}/C_{areal}$ [ $\Omega/\frac{mAh}{cm^2}$ ]	$\tau$ [—]	$R_{ct}$ [ $\Omega$ ]	$R_{ct} \times C_{areal}$ [ $\Omega \frac{mAh}{cm^2}$ ]	$R_{ct}/R_{ion}$ [—]	Impedance regime
7.5	36.3	4.8	7.7	2.27	17.3	0.06	transport limited
2.9	13.7	4.7	7.5	5.01	14.5	0.37	transition regime
1.5	6.70	4.5	7.1	8.70	13.1	1.30	kinetically limited
0.6	2.80	4.7	7.7	16.2	9.7	5.79	kinetically limited

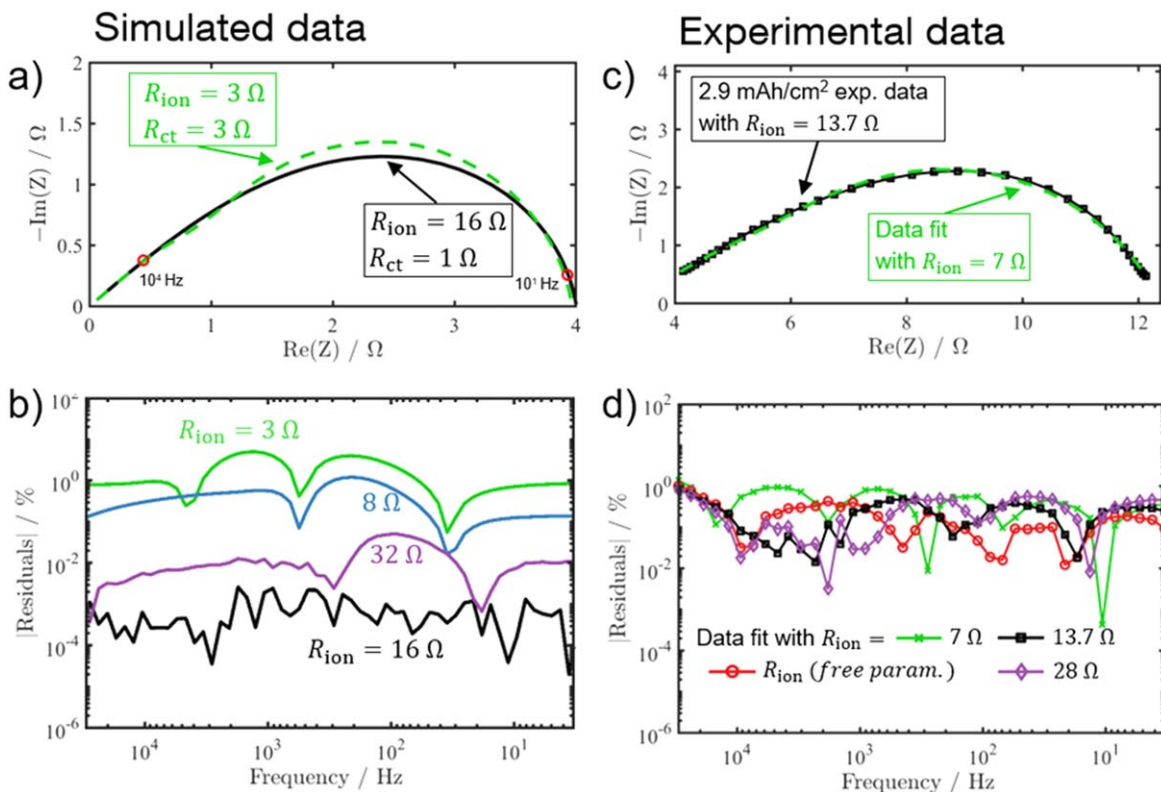


**Figure 7.** Comparison of impedance fits of simulated and of experimental impedance spectra. (a) Simulated impedance data calculated from Eq. 1 with  $R_{\text{ion}} = 16 \Omega$ ,  $R_{\text{ct}} = 1 \Omega$ ,  $Q_{\text{dl}} = 2 \text{ mF}$ , and  $\alpha = 0.9$  (corresponding to the transport limited spectrum, black line). The green dashed spectrum was fitted using Eq. 1 while keeping  $R_{\text{ion}}$  fixed to  $3 \Omega$ , resulting in a fitted value of  $R_{\text{ct}} = 3 \Omega$  (i.e.,  $R_{\text{ct}}/R_{\text{ion}}$  indicates the kinetically limited regime) of the simulated spectrum (black curve in a) when fixing  $R_{\text{ion}}$  to the different values marked in the figure. (c) Experimental data of the  $2.9 \text{ mAh cm}^{-2}$  electrode (black squares; data taken from Fig. 2d), fitted with a fixed value of  $R_{\text{ion}} = 7 \Omega$  (green dashed line) that is 2-fold lower than the value determined under blocking conditions ( $13.7 R_{\text{ion}}$ ). (d) Residuals of the fit in c (green line) as well as the residuals for various fixed values of  $R_{\text{ion}}$  that differ by factors of 2 from the value determined under blocking conditions. That the residuals are within the same range for all fits (indicating the same quality of fit) highlights the difficulty when fitting experimental spectra without the prior determination of  $R_{\text{ion}}$ .

different fixed  $R_{\text{ion}}$  values that are centered around the  $R_{\text{ion}}$  value obtained under blocking conditions, illustrating that the fit quality is essentially independent of the chosen  $R_{\text{ion}}$  value, while resulting in different values of  $R_{\text{ct}}$ ,  $Q_{\text{dl}}$ , and  $\alpha$ . This demonstrates that  $R_{\text{ion}}$  must be known when trying to extract  $R_{\text{ct}}$  values from impedance spectra in the transition or the transport limited regime.

Figure 7a shows a simulated porous electrode impedance spectrum in the transport limited regime (black line), calculated from Eq. 1 with  $R_{\text{ion}} = 16 \Omega$ ,  $R_{\text{ct}} = 1 \Omega$ ,  $\alpha = 0.9$ , and  $Q_{\text{dl}} = 2 \text{ mF}$  (note that the main difference to the simulated spectrum for  $R_{\text{ion}} = 16 \Omega$  and  $R_{\text{ct}} = 1 \Omega$  in Figs. 2a/2b (orange lines) is that here a more realistic value of  $\alpha = 0.9$  was chosen). The green dashed line shows a spectrum fitted to the black spectrum where  $R_{\text{ion}}$  is fixed falsely to a much lower value of  $3 \Omega$ , giving the remaining parameters best fitted to be  $R_{\text{ct}} \approx 3.0 \Omega$ ,  $\alpha \approx 0.90$ , and  $Q_{\text{dl}} \approx 0.35 \text{ mF}$ , which would correspond to a spectrum in the kinetically limited regime (i.e.,  $R_{\text{ct}}/R_{\text{ion}} < 0.62$ , see Fig. 4c). The Nyquist plot representing this fit (green dashed line) overlaps closely for higher ( $>10^4 \text{ Hz}$ , left side of the spectrum) and lower frequencies ( $<10^1 \text{ Hz}$ , right side), but deviates visibly at intermediate frequencies.

To better quantify the differences between the simulated spectrum (black line) and the spectra fitted with different fixed  $R_{\text{ion}}$  values, Fig. 7b shows the magnitude of the residuals vs frequency, i.e., the scaled difference between the simulated data and fit vectors  $\left( \frac{|Z(f_i)| - |Z_{\text{fit}}(f_i)|}{|Z_{\text{fit}}(f_i)|} \right)$  at the same frequency  $f_i$  (in %). The thus determined residuals for the fit with a fixed  $R_{\text{ion}} = 3 \Omega$  (green line in Fig. 7b) are a quantitative measure of the difference between the

simulated spectrum (black line in Fig. 7a) and the thus fitted spectrum (dashed green line in Fig. 7a), with maximum values of the residuals of  $\sim 5\%$ . A sudden dip in residuals followed by a semi-circle shaped features (e.g., between  $10^4$  to  $10^2 \text{ Hz}$  for the green line in Fig. 7b) are points where the fitted spectrum deviates from the simulated/experimental data over wider frequency ranges. Ideally, a perfectly fitted spectrum gives low residuals which can be described as noise around the fitted datapoints, whereas constant deviations over a wider frequency range can be the result of more systematic errors in the analysis (as seen, e.g., in the green residuals).

As expected, fitting the data using the correct  $R_{\text{ion}}$  value (i.e., fixing  $R_{\text{ion}} = 16 \Omega$  while fitting) gives the lowest residuals ( $\sim 10^{-3}\%$ ; see black line in Fig. 7b) and yields the correct values for  $R_{\text{ct}}$ ,  $\alpha$ , and  $Q_{\text{dl}}$  (i.e., the values that were used to generate the simulated spectrum). Since the simulated spectrum can be described as transport limited ( $R_{\text{ct}}/R_{\text{ion}} \ll 0.21$ , see Fig. 4c), fixing  $R_{\text{ion}}$  to  $32 \Omega$  (purple line in Fig. 7b) and fitting the simulated spectrum still gives very low residuals ( $\sim 10^{-2}\%$ ). In this case, the fit gives values for  $R_{\text{ct}}$  of  $0.5 \Omega$ ,  $\alpha \approx 0.9$ , and  $Q_{\text{dl}} \approx 1 \text{ mF}$  (i.e., a 2-fold lower  $R_{\text{ct}}$  value, as expected from the discussion of the spectra in Fig. 2), showing that while these two transport limited spectra (i.e., for  $R_{\text{ion}} = 16 \Omega$  and for  $R_{\text{ion}} = 32 \Omega$ ) are theoretically not identical, they very closely match each other. Fitting the simulated spectrum with a lower fixed  $R_{\text{ion}}$  value of  $8 \Omega$  still gives reasonably small residuals on the order of 1% (with  $R_{\text{ct}} \approx 1.9 \Omega$ ,  $Q_{\text{dl}} \approx 0.95 \text{ mF}$ , and  $\alpha \approx 0.9$ ), suggesting that the spectrum is in the transition region ( $R_{\text{ct}}/R_{\text{ion}} \approx 0.48$ , see Fig. 4c). In summary, while the fit of simulated, perfectly noise-free impedance data in the transport controlled regime would still yield the correct

values of  $R_{\text{ion}}$ ,  $R_{\text{ct}}$ ,  $Q_{\text{dl}}$ , and  $\alpha$ , the residuals that are obtained when fixing an  $R_{\text{ion}}$  value that is different by a factor of 2 are still very small (below 1%). Therefore, owing to the noise in experimental impedance data, a unique fitting result cannot any more be obtained, as will be illustrated in the following.

Figure 7c shows the experimentally obtained impedance spectrum for the electrode with an areal capacity of  $2.9 \text{ mAh cm}^{-2}$  (black squares; same data as in Fig. 2c) to 3 Hz, since datapoints below 3 Hz are dominated by diffusion phenomena. Based on the  $R_{\text{ion}}$  value of  $13.7 \Omega$  that was determined for the pristine electrode under blocking conditions (see Fig. 2d), the fit of the impedance spectrum using Eq. 1 (with an additional resistance element in series for the high frequency separator resistance) and fixing  $R_{\text{ion}}$  at  $13.7 \Omega$  yields  $R_{\text{ct}} = 5.0 \Omega$  (also  $Q_{\text{dl}} = 1.35 \text{ mF}$  and  $\alpha = 0.78$ , see Table III). Thus, based on  $R_{\text{ct}}/R_{\text{ion}} \approx 0.36$ , this impedance spectrum fit suggests that the impedance response of this electrode falls within the transition regime (see Fig. 4c). As shown in Fig. 7d (black squares), the residuals for this fit are at  $\leq 1\%$  over the entire frequency range. On the other hand, if  $R_{\text{ion}}$  is treated as a fitting parameter (i.e., the software was allowed to alter all four parameters to find the best fit, an approach that would be used if  $R_{\text{ion}}$  was unknown), the fitted values are  $R_{\text{ion}} = 11.0 \Omega$  and  $R_{\text{ct}} = 5.7 \Omega$  (also  $Q_{\text{dl}} = 1.1 \text{ mF}$  and  $\alpha = 0.78$ ). Based on  $R_{\text{ct}}/R_{\text{ion}} \approx 0.52$ , the impedance spectrum still falls within the transition regime. The maximum residuals (red circles) are also  $\leq 1\%$  and thus essentially identical with those obtained when using the  $R_{\text{ion}}$  value determined for the pristine electrode under blocking conditions.

Fitting the experimental spectrum using an  $R_{\text{ion}}$  value that is arbitrarily fixed to  $7.0 \Omega$  results in a spectrum that is represented by the green dashed line in Fig. 7c. The corresponding fitted value of  $R_{\text{ct}}$  is now  $7.0 \Omega$  (also  $Q_{\text{dl}} = 1 \text{ mF}$  and  $\alpha = 0.71$ ), i.e., the spectrum can now be described as kinetically limited, since  $R_{\text{ct}}/R_{\text{ion}} \approx 1$ . The residuals for this fit (green crosses in Fig. 7d) are also  $\leq 1\%$  over the entire frequency range and only marginally higher than for the fits where  $R_{\text{ion}}$  is either fixed at the value obtained for the pristine electrode under blocking conditions or where  $R_{\text{ion}}$  is treated as a fitting parameter (see above). Fixing  $R_{\text{ion}}$  at  $28 \Omega$ , i.e., at a 2-fold higher value than suggested by the blocking condition measurements, also yields residuals of  $\leq 1\%$  (purple diamonds); with the fitted  $R_{\text{ct}}$  value of  $2.9 \Omega$  (also  $Q_{\text{dl}} = 3.3 \text{ mF}$  and  $\alpha = 0.76$ ), the impedance response of the electrode would now fall into the transport limited regime ( $R_{\text{ct}}/R_{\text{ion}} \approx 0.11$ , see Fig. 4c).

The above analysis illustrates that a fit of the impedance spectrum of a graphite electrode with a pore resistance that is similar in value to the charge transfer resistance, as is the case for large areal capacitances (i.e., for areal capacitances of near/above  $3 \text{ mAh cm}^{-2}$ ), does not allow for a reliable determination of  $R_{\text{ct}}$ , since the difference in the residuals is rather negligible. For example, for the  $2.9 \text{ mAh cm}^{-2}$  graphite electrode examined here, assuming  $R_{\text{ion}}$  values between  $7\text{--}28 \Omega$  yields essentially identical residuals, while the fitted  $R_{\text{ct}}$  values differ by a factor of  $\sim 2.5$  ( $2.9\text{--}7 \Omega$ ). The low  $\alpha$ -value of real electrodes also plays a role in this, since the transition between the straight line at high frequencies (having slope of  $45^\circ \times \alpha$ ) to the depressed semi-circle feature is a less pronounced feature for lower  $\alpha$ -values. This is seen in the impedance fit for a fixed  $R_{\text{ion}}$  of  $7 \Omega$  (green dashed line in Fig. 7c), where the fit gives an  $\alpha$ -value of  $0.71$  compared to  $0.78$  when using the  $R_{\text{ion}}$  value of  $13.7 \Omega$  that is obtained under blocking conditions. Lowering the  $\alpha$ -value makes for a more seamless transition between the initial straight line feature to the depressed semi-circle, making it difficult to distinguish it from a spectrum with a higher  $R_{\text{ion}}$ . Therefore, in view of the inevitable noise in experimental impedance spectra, the quantification of  $R_{\text{ct}}$  from the impedance spectra of high areal capacity graphite electrodes requires an independent measurement of  $R_{\text{ion}}$ , which, as shown here, can be obtained under blocking conditions for a pristine electrode. While the thus determined  $R_{\text{ion}}$  may increase over extended charge/discharge cycling, it is expected to remain constant over the first few cycles.<sup>21</sup>

## Conclusions

This work shows how the ratio of the charge transfer resistance to the resistance stemming from the electrolyte filled porous path inside a porous electrode ( $R_{\text{ct}}/R_{\text{ion}}$ ) influences the electrode impedance spectra of Li-ion battery electrodes. We use a simplified transmission line model (TLM) with the ionic resistance  $R_{\text{ion}}$  in the electrolyte and the faradaic reaction charge transfer resistance  $R_{\text{ct}}$  as the only contributions to the spectrum, neglecting the electronic resistance of the solid phase or diffusion resistances in both the electrolyte and in the solid phase that only appear at very low frequencies, to model the influence of areal capacity (or mass loading) on the spectrum shape and the low-frequency resistance  $L$ .

Simulating changes in electrode loading by considering that  $R_{\text{ct}} \propto \frac{1}{C_{\text{areal}}}$  and  $R_{\text{ion}} \propto C_{\text{areal}}$ , the porous electrode impedance spectra show a change in shape when changing the ratio  $\vartheta \equiv R_{\text{ct}}/R_{\text{ion}}$ . For  $\vartheta \gg 1$ , the electrode is described as *kinetically limited* and the impedance spectrum is dominated by a semicircle that represents  $R_{\text{ct}}$ . For  $\vartheta \ll 1$ , the electrode is described as *transport limited*, where any change in active material loading barely affects the shape of the impedance spectra and where the low-frequency intercept becomes practically independent of the active material loading. Hence the transport limited regime requires prior knowledge of  $R_{\text{ion}}$  to quantify  $R_{\text{ct}}$  from an impedance fit.

We then provide practical boundaries to describe the kinetically and transport limited regime. For  $\vartheta \geq 0.62$ , the electrode impedance can be calculated as  $L = R_{\text{ct}} + \frac{R_{\text{ion}}}{3}$ , whereas for  $\vartheta \leq 0.21$ , the electrode is transport limited and the low-frequency electrode resistance is described by the  $L = \sqrt{R_{\text{ion}}R_{\text{ct}}}$ . For in-between values of  $\vartheta$ , no simplified solution can be determined. The loading independent impedance spectra for transport limited electrodes is explained by the limited measurement penetration depth (smaller than the thickness of the electrode). As  $R_{\text{ion}}$  becomes dominating, only the electrode side close to the separator contributes to the measurement, and thus parts of the electrode (near the current collector) are invisible to the measurement. The findings of the simulation were confirmed by experimentally obtained impedance spectra of graphite electrodes of different areal capacities. Graphite electrodes between  $0.6\text{--}7.5 \text{ mAh cm}^{-2}$  were measured and found to be ranging from kinetically limited to transport limited.

To analyze the impedance spectra without prior knowledge of its limitation (i.e., transport vs kinetically limited electrodes), we provide a tool and a step by step description of a porous electrode impedance analysis without the need for a fitting software. This analysis requires measurement of the pore resistance under blocking conditions to accurately determine the charge transfer resistance from impedance measurements. While analyzing transport limited electrodes (in non-blocking conditions), care should be taken in interpreting the values of charge transfer resistance values obtained from this analysis, since the measurement of  $R_{\text{ct}}$  is obtained only by partial probing of the electrode (due to the limited signal penetration depth). The impedance of an electrode having an inhomogeneous distribution of charge-transfer resistance (i.e., in the transport limited regime) will only provide information of the charge transfer resistance that lies within the penetration depth. An analysis of graphite electrodes with widely varying areal capacities showed that our assumption of a direct proportionality of  $R_{\text{ion}}$  with electrode loading holds true. On the other hand, experimentally observed relationship between  $R_{\text{ct}}$  and areal capacity deviated somewhat from the assumed inverse proportionality of  $R_{\text{ct}}$  with areal capacity. Possibilities for such a deviation could be the local probing of the electrode when its response becomes transport limited or might arise from the more inhomogeneous formation of a transport limited electrode.

Lastly, we show that fitting simulated spectra (devoid of any noise) of transport limited electrodes without prior knowledge of their pore resistance is theoretically possible and results in the

extraction of the correct parameters. However, the differences between simulated transport limited impedance spectra (simulating changes in loading/areal capacity) are minute. The fits of experimentally obtained spectra of transport limited electrodes or those in the transition region are practically indistinguishable from other transport limited spectra, highlighting the need for the separate measurement of  $R_{ion}$ .

### Acknowledgments

R. M. gratefully acknowledges the funding by BMW AG. J. K. and B. S. acknowledges the financial support from the BMBF (Federal Ministry of Education and Research, Germany), under the auspices of the ExZellTUM II and III projects (grant numbers 03XP0081 and 03XP0255). We would also like to thank Johannes Landesfeind for valuable discussions and Maximilian Graf for providing the cross section porous electrode image.

### Appendix

The section below describes the mathematical background for the current distribution analysis shown in Fig. 3.

Figure A-1 shows the equivalent circuit for which we write the charge conservation equation for the electrolyte phase:

$$\left( \frac{\mathbf{E}}{\hat{r}_{ct}} \right) = -\nabla \cdot (-\kappa_{eff} \nabla E) \quad [A.1]$$

$[A \cdot m^{-3}]$                        $[A \cdot m^{-2}]$   
 $[A \cdot m^{-3}]$                        $[A \cdot m^{-3}]$

The right-hand side represents the change in the flux of ionic current, whereas the left-hand side represents the current due to the charge transfer reaction. Here  $E$  [V] is the potential in the time domain,  $\hat{r}_{ct}$  [ $\Omega m^3$ ] is the charge transfer resistance of the small volume element, and  $\kappa_{eff}$  is the effective conductivity of the electrolyte. Since we are dealing with a 1-dimensional system, Eq. A.1 can be simplified. We take the Laplace transform and the resulting Eqn. is shown in Eq. A.2:

$$\frac{\mathbf{E}}{\hat{r}_{ct}} = \kappa_{eff} \frac{d^2 \mathbf{E}}{dX^2} \quad [A.2]$$

where  $X$  [m] is the axial direction going from 0 to the thickness of the electrode  $d$  [m]. Introducing  $x = X/d$ , we get the following equation:

$$\frac{\mathbf{E}}{\hat{r}_{ct}} = \frac{\kappa_{eff}}{d^2} \frac{d^2 \mathbf{E}}{dx^2} \quad [A.3]$$

Rearranging Eq. A.3 to introduce the total charge transfer resistance ( $R_{ct}$ ) and the ionic resistance ( $R_{ion}$ ) as follows:

$$\mathbf{E} = \frac{\hat{r}_{ct}}{d} \frac{A}{A} \frac{\kappa_{eff}}{d} \frac{d^2 \mathbf{E}}{dx^2} \quad [A.4]$$

Notice that  $\frac{\hat{r}_{ct}}{Ad} = R_{ct}$  [ $\Omega$ ] and  $\frac{A \kappa_{eff}}{d} = \frac{1}{R_{ion}}$ , whereby  $A$  is the geometric area. We get Eq. A.5 as a second-order differential equation:

$$\mathbf{E} = \frac{R_{ct}}{R_{ion}} \frac{d^2 \mathbf{E}}{dx^2} = \vartheta \frac{d^2 \mathbf{E}}{dx^2} \quad [A.5]$$

To solve Eq. A.5, the two boundary conditions in the Laplace domain are:  $\mathbf{E}(x=0) = 1$  and  $\left. \frac{d\mathbf{E}}{dx} \right|_{x=1} = 0$  (no electrolyte current leaves the current collector). We then introduce  $\vartheta = \frac{R_{ct}}{R_{ion}}$ , to make

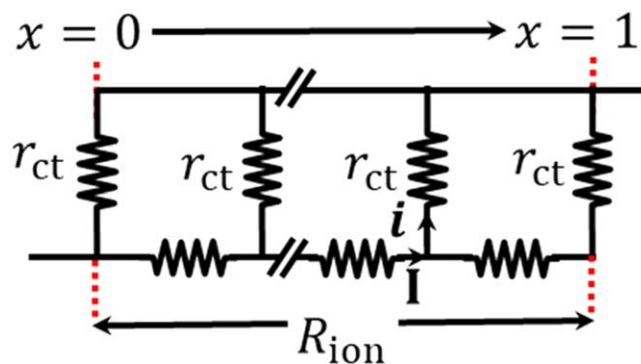


**Figure A1.** Simplification of the transmission line model presented in Fig. 1 for the case when the frequency is sufficiently low so that the current contributed by the double layer capacitance becomes negligible. Note that this TLM also excludes the effect of diffusion of lithium in electrolyte and solid phase that becomes significant at very low frequencies. Only the charge transfer reaction acts as a source or a sink for the current, the double-layer capacitance is inactive at such a low frequency.

the expression more compact. The solution to Eq. A.5 with the above specified boundary conditions can be expressed as follows (a modified version of Eq. A.6 can be found in Lasia, chapter 9):

$$\mathbf{E} = \frac{\cosh((1-x)/\sqrt{\vartheta})}{\cosh(1/\sqrt{\vartheta})} \quad [A.6]$$

From Eq. A.6, we get the following equation for the current in the pore of the porous electrode (using Ohm's law for electrolyte):

$$\mathbf{I} = -\frac{1}{R_{ion}} \frac{d\mathbf{E}}{dx} = \frac{1}{R_{ion} \sqrt{\vartheta}} \frac{\sinh((1-x)/\sqrt{\vartheta})}{\cosh(1/\sqrt{\vartheta})} \quad [A.7]$$

Here  $\mathbf{I}$  is the complex current in the pore,  $x$  is the axial coordinate in the direction of the electrode thickness going from the separator/electrode interface ( $x=0$ ) to the electrode/current collector interface ( $x=1$ ). We then define the complex current density  $i(x) = -d\mathbf{I}/dx$ , which represents the change in current at any point (due to charge transfer reaction only, as we have specified that the frequency is zero). A uniform  $i(x)$  will mean a uniform reaction and a full utilization of the electrode.

$$i(x) = -\frac{d\mathbf{I}}{dx} = \frac{1}{R_{ct}} \frac{\cosh((1-x)/\sqrt{\vartheta})}{\cosh(1/\sqrt{\vartheta})} \quad [A.8]$$

Finally, we define the scaled complex current density as the current density scaled with the current density at  $x=0$ :

$$i_s(x) = \frac{i(x)}{i|_{x=0}} = \frac{\cosh((1-x)/\sqrt{\vartheta})}{\cosh(1/\sqrt{\vartheta})} \quad [A.9]$$

The scaled current density at the current collector can be calculate by substituting  $x=1$ , in Eq. A.9.

$$i_s(x=1) = \frac{1}{\cosh(1/\sqrt{\vartheta})} \quad [A.10]$$

During charging, all electrodes attained their full capacity at the cutoff of 40 mV vs  $Li^+/Li$  with the exception of the 7.5 mAh  $cm^{-2}$  electrode which reached  $\sim 5.6$  mAh  $cm^{-2}$  due to the exceptionally high loading. During discharge, all electrodes reach the previously charged capacity as the measurement is conducted as a half-cell with a Li-FSG counter electrode.

## List of Symbols

Symbol	Description [unit]
$A$	Geometric area [m <sup>2</sup> ]
$\alpha$	Constant phase exponent [–]
$C$	Arbitrary capacitance value
$C_{dl}$	Double layer capacitance [F]
$\delta_j$	Loading unit ( $\delta_2 = 2 \times \delta_1$ and $\delta_3 = 3 \times \delta_1$ ) [–]
$d$	Thickness of the electrode [m]
$E$	Potential (time domain) [V]
$\mathbf{E}$	Complex potential (Laplace domain) [V]
$\vartheta$	Ratio of charge-transfer to ionic resistance ( $R_{ct}/R_{ion}$ ) [–]
$\vartheta_{approx}$	Approximated $\vartheta$ using simplified expressions [–]
$\vartheta_{true}$	True $\vartheta$ using full solution [–]
$\varepsilon$	Porosity of the electrode [–]
$\varepsilon_\vartheta$	Error in approximating $\vartheta$ [–]
$f$	Frequency [Hz]
$f_{peak}$	Peak frequency, where the imaginary resistance attains its peak value [Hz]
$\hat{f}_{peak}$	Scaled peak frequency [–]
$\mathbf{I}$	Complex current in Laplace domain [A]
$i$	Complex current density ( $= -d\mathbf{I}/dx$ ) in Laplace domain [A]
$i_s$	Scaled complex current density ( $i(x)/i _{x=0}$ ) in Laplace domain [–]
$Im_{peak}$	Peak value of the imaginary resistance [ $\Omega$ ]
$j$	Imaginary unit
$\kappa$	Conductivity of the bulk electrolyte [S/m]
$\kappa_{eff}$	Effective conductivity of electrolyte in porous media ( $\kappa_{eff} = \kappa\varepsilon/\tau$ ) [S/m]
$L$	Difference between low and high frequency intercept [ $\Omega$ ]
$Q_{dl}$	Double layer constant phase element capacitance of entire electrode [ $Fs^{1-\alpha}$ ]
$q_{dl}$	Double layer constant phase element capacitance of electrode segment [ $Fs^{1-\alpha}$ ]
$R$	Arbitrary resistance value
$R_{ion}$	Ionic resistance ( $=d/(A\kappa_{eff})$ ) [ $\Omega$ ]
$r_{ion}$	Ionic resistance of a small element in the TLM [ $\Omega$ ]
$R_{ct}$	Charge-transfer resistance of an entire electrode [ $\Omega$ ]
$r_{ct}$	Charge-transfer resistance of a small element in the TLM [ $\Omega$ ]
$\hat{r}_{ct}$	Charge-transfer resistance of a small volume element ( $=R_{ct}Ad$ ) [ $\Omega m^3$ ]
$\tau$	Tortuosity of the electrode [–]
$\omega$	Angular frequency ( $=2\pi f$ ) [ $Rad\ s^{-1}$ ]
$x$	Scaled axial length [–]
$X$	Axial coordinate [m]
$\mathbf{Z}$	Complex impedance [ $\Omega$ ]
<b>Descriptive subscripts:</b>	
AM	Active Material
Areal	Relating to the geometric area

Fit	Parameter obtained by a spectrum fit
true	Parameter $\vartheta$ obtained using the full impedance solution (Eq. 2)
approx	Parameter $\vartheta$ obtained using the simplified solution (Eqs. 4 and 5)
peak	Relating to the peak of the “semicircle”
eff	Relating to the effective parameter
dl	Relating to the double layer capacitance
G	Relating to the graphite active material
ion	Relating to the ionic resistance
ct	Relating to the charge transfer resistance
s	Scaled parameter

## ORCID

Robert Morasch  <https://orcid.org/0000-0002-9931-1022>  
 Josef Keilhofer  <https://orcid.org/0000-0002-5092-1567>  
 Hubert A. Gasteiger  <https://orcid.org/0000-0001-8199-8703>  
 Bharatkumar Suthar  <https://orcid.org/0000-0002-8612-9483>

## References

1. A. Zaban, E. Zinigrad, and D. Aurbach, *J. Phys. Chem.*, **100**, 3089 (1996).
2. M. Ender, A. Weber, and E. Ivers-Tiffée, *Electrochem. Commun.*, **34**, 130 (2013).
3. M. Cronau, M. Kroll, M. Szabo, F. Sälzer, and B. Roling, *Batter. Supercaps.*, **3**, 611 (2020).
4. J. Huang and J. Zhang, *J. Electrochem. Soc.*, **163**, A1983 (2016).
5. N. Meddings et al., *J. Power Sources*, **480**, 228742 (2020).
6. D. Schreiner et al., *J. Electrochem. Soc.*, **168**, 030507 (2021).
7. J.-H. Schunemann, H. Dreger, H. Bockholt, and A. Kwade, *ECS Trans.*, **73**, 153 (2016).
8. N. Ogihara, S. Kawauchi, C. Okuda, Y. Itou, Y. Takeuchi, and Y. Ukyo, *J. Electrochem. Soc.*, **159**, A1034 (2012).
9. N. Ogihara, Y. Itou, T. Sasaki, and Y. Takeuchi, *J. Phys. Chem. C*, **119**, 4612 (2015).
10. N. Ogihara and Y. Itou, *R&D Rev. Toyota CRDL*, **48**, 17 (2017).
11. Y. Itou, N. Ogihara, and S. Kawauchi, *J. Phys. Chem. C*, **124**, 5559 (2020).
12. A. N. Mistry and P. P. Mukherjee, *Phys. Chem. Chem. Phys.*, **21**, 3805 (2019).
13. S. Solchenbach, D. Pritzl, E. J. Y. Kong, J. Landesfeind, and H. A. Gasteiger, *J. Electrochem. Soc.*, **163**, A2265 (2016).
14. R. Morasch, B. Suthar, and H. A. Gasteiger, *J. Electrochem. Soc.*, **167**, 100540 (2020).
15. A. Lasia, “Electrochemical Impedance Spectroscopy and its Applications.” *Modern Aspects of Electrochemistry* (Springer, Boston, MA) 32, p. 1 (2002).
16. S. G. Compton, S. G. Beesley, and D. A. Jones, *Heredity (Edinb.)*, **61**, 235 (1988).
17. J. Landesfeind, M. Ebner, A. Eldiven, V. Wood, and H. A. Gasteiger, *J. Electrochem. Soc.*, **165**, A469 (2018).
18. I. V. Thorat, D. E. Stephenson, N. A. Zacharias, K. Zaghbi, J. N. Harb, and D. R. Wheeler, *J. Power Sources*, **188**, 592 (2009).
19. J. Landesfeind, J. Hattendorff, A. Ehrl, W. A. Wall, and H. A. Gasteiger, *J. Electrochem. Soc.*, **163**, A1373 (2016).
20. J. Landesfeind, D. Pritzl, and H. A. Gasteiger, *J. Electrochem. Soc.*, **164**, A1773 (2017).
21. D. Pritzl, J. Landesfeind, S. Solchenbach, and H. A. Gasteiger, *J. Electrochem. Soc.*, **165**, A2145 (2018).
22. P. Lu, C. Li, E. W. Schneider, and S. J. Harris, *J. Phys. Chem. C*, **118**, 896 (2014).
23. J. H. Kim, S. J. Lee, J. M. Lee, and B. H. Cho, *7th International Conference on Power Electronics, ICPE'07*(IEEE, Piscataway, NJ) p. 1173 (2007).
24. S. Zhao, F. Wu, L. Yang, L. Gao, and A. F. Burke, *Electrochem. Commun.*, **12**, 242 (2010).
25. T. Waldmann, B. I. Hogg, and M. Wohlfahrt-Mehrens, *J. Power Sources*, **384**, 107 (2018).
26. M. Doyle, T. F. Fuller, and J. Newman, *J. Electrochem. Soc.*, **140**, 1526 (1993).
27. J. Landesfeind and H. A. Gasteiger, *J. Electrochem. Soc.*, **166**, A3079 (2019).
28. S. Jaiser, J. Kumberg, J. Klaver, J. L. Urai, W. Schabel, J. Schmatz, and P. Scharfer, *J. Power Sources*, **345**, 97 (2017).
29. R. Morasch, J. Landesfeind, B. Suthar, and H. A. Gasteiger, *J. Electrochem. Soc.*, **165**, A3459 (2018).